Software Tool for Brain Connectivity Analysis

by
Gan Heng Yi
18190

Dissertation submitted in partial fulfilment of
the requirements for the
Bachelor of Engineering (Hons)
(Electrical and Electronics)

JANUARY 2017

Universiti Teknologi PETRONAS
Bandar Seri Iskandar
31750 Tronoh
Perak Darul Ridzuan

CONTENTS

TABLE OF FIGURES

CERTIFICATION OF APPROVAL

Software Tool for Brain Connectivity Analysis

By

Gan Heng Yi

18190

A project dissertation submitted to the

Department of Electrical & Electronics Engineering

Universiti Teknologi PETRONAS

in partial fulfilment of the requirement for the

Bachelor of Engineering (Hons)

(Electrical & Electronics Engineering)

Approved by,

_____

Dr HO TATT WEI

UNIVERSITI TEKNOLOGI PETRONAS

TRONOH, PERAK

January 2017

CERTIFICATION OF ORIGINALITY

This is to certify that I am responsible for the work submitted in this project, that the original work is my own except as specified in the references and acknowledgements, and that the original work contained herein have not been undertaken or done by unspecified sources or persons.

_____

GAN HENG YI

ABSTRACT

Structural magnetic resonance imaging (MRI) is a constitutive part of the clinical assessment of neurodegenerative patients. The routine neuroimaging evaluation of structural markers from preclinical to conspicuous stage is a key figure of how the disease is conceptualized, and will determine its imminent diagnosis and treatment to dementia. Atrophy, a late feature in the progression of the disease, is now a valid diagnostic marker to the neurodegenerative diseases. At the mild cognitive impairment stage of the Alzheimer disease (AD), the valid diagnostic marker is the atrophy of medical temporal structure [33]. In temporal lobe epilepsy (TLE), the atrophy of the subcortical brain structures specifically the size of the hippocampus is observed [34]. Apart from these neurodegenerative diseases, there is a significant evidence showing that the long-term 'Ketum' drug abuse also causes dementia which are profound impairments of learning and memory. These cognitive-impairing effects are revealed by the analysis of electroencephalogram (EEG) that shows a significant decline of delta power in the hippocampus [35]. Additionally, in the electrocorticography (ECoG) of the frontal cortex, it is found out that there is a complete suppression of the delta and theta bands [35]. Nonetheless, it is unclear whether it has a potential biomarker, just like AD and TLE have. Even if there is an evidence that shows the location of biomarker that can relate the atrophy by utilizing the conventional MRI technique based on diffusion-weighted imaging (DWI), it is unknown whether the cause of this atrophy is due to local degeneration of the nerve cells or caused by degeneration of the nerve connections or both. In this paper, a standardized protocol of white matter (WM) tractography is presented to reconstruct the highly directional architecture of the WM of the brain tissues based on a recent prominent approach of MRI technique, called diffusion tensor imaging (DTI). It also includes the development of integral visualization of 3D WM geometry and structure with the 2D T1-weighted (T1W) images to investigate the status of the local degeneration of neurons in the Grey Matter (GM) with the effect of the drug addiction. Further, observational study of the WM of two-sample subjects is created as the complement to enhance the evidence of biomarker potential, by reflecting the value in differential diagnosis. Utmost importance, Tract-Based Spatial Statistics (TBSS) [52] is incorporated to study the local degeneration of fiber tracks of the drug addicted subjects, and to investigate the subcortical regions that encounters this anatomical distribution of WM microstructural damage.

ACKNOWLEDGEMENT

Foremost, a profuse thanks to my supervisor Dr. Eric Ho Tatt Wei that has provided me his consistent guidance and support in assisting me to complete my Final Year Project. His patience in sharing me his experience and knowledge is unforgettable especially to the person like me who is a complete novice in bio-neuroimaging field at the beginning of the project. Next, I feel thankful to the professional expertize that developed the DIPY library and FSL tool. Without them, the path to success and completion of this project is difficult. Last but not least, a great appreciation towards Universiti Sains Malaysia (USM) that provides me the datasets of healthy subjects and 'Ketum' drug addiction subjects.

1.0 INTRODUCTION

1.1 Background

In analogy to the electrical cable in electrical communication system, White Matter (WM) in the human brain is the transmission medium of the neurotransmission. Through the WM, the neurons communicate with each other by sending electrical impulses. These neurons spread on the surface of the brain and are referred to Grey Matter (GM). Damage to the WM and GM in the brain can result dementia. The dementia is the condition of the decline in brain cognitive functions. There includes the varying degree of memory loss, difficulty with problem solving, poor coordination and motor functions, and so on.

The major root cause to the dementia is the neurodegenerative diseases. The neurodegenerative diseases are incurable. Since the neurons normally do not reproduce themselves, they are irreplaceable if they are damaged or die. And many of the neurodegenerative diseases are related to the progressive degeneration of neurons. Examples of neurodegenerative diseases are Alzheimer's, Huntington's, and Parkinson's disease. Apart from the neurodegenerative diseases, according to the preclinical study from University Sains Malaysia (USM), overdose and addiction to mitragynine coming from the plant 'Ketum' also poses dementia [35].

Early and accurate differential diagnosis of dementia can increase the likelihood of successful treatment. The sooner the diagnosis of the dementia is confirmed, the more effective the treatment of the reversible conditions. Even though some symptoms of the dementia are not reversible, the prompt treatments can slow or stop the rate of further cognitive decline of brain functions. Structural imaging based on magnetic resonance is crucial to clinician assessment of data acquisition to earlier diagnosis when the cognitive symptoms are first noticed.

The current guidelines recognize the structural brain imaging along with a range of laboratory test to be the early diagnostic evaluation of patients with dementia [36]. The conventional MRI imaging is widely used as the diagnostic criteria for its remarkable presentation of the imaging markers [37]. It includes T1-weighted (T1W) gadolinium (Gd) enhanced and spin-echo T2-weighted imaging (T2W) scans. Nevertheless, it exists a

major drawback of the insufficient information of underlying neurodegenerative changes in grey-white brain tissue contrast picture [37], and the presented biomarkers are not always sufficiently overt to meet the clinical criteria for differential diagnosis.

As the new neuroimaging approach, diffusion tensor imaging (DTI) is a sophisticated MRI technique that offers the information about the WM integrity. It is based on the anisotropic water diffusion to characterize the axonal connectivity of the brain network tropology in color maps. To reconstruct the neuronal tracts into 3D models from the eigenvector color maps, the technique is called the WM tractography. Owing to its clear and unique characterization of the microstructure and physiological information regarding to the WM tissues, it is a robust neuroimaging acquisition and analysis methods utilized for clinical, neuropsychological, and neuroimaging assessments.

Studying the macroscopic axonal organization for brain structural connectivity with the DTI methodologies intensifies the value of imaging markers in the early diagnosis of neurodegenerative diseases. Any loss of axonal tracts that is discovered enables the locations of atrophy being identified as unusual biological events of interest occur. The examination of the axonal anatomy between the healthy and disease states reflects a new potential useful clinical assessment in structural imaging.

However, tracking the axons that communicating with each other of more than 100 billion neurons is an impractical way to examine the marker from the entire brain. The series of steps in WM tractography, segmentation and clustering is labor-intensive, despite of the result intensifies the value of imaging marker. The complexity is another concern. Manual delineation of region of interest based on the tractography datasets is a widely-used approach in the research studies to reconstruct the pathways of interest and to investigate the pathological conditions, yet it is a great challenge to whom without extensive anatomical expertise.

Simplification is the general preference of clinical assessment to obtain the result. Protocol standardization and automation in WM tractography to reconstruct the 3D geometric and structural WM nerve fibers is of crucial importance. Attempts to develop an integral visualization that incorporates the T1W with DTI structural imaging are incremental to the diagnostic significance in locating any unusual biological marker in

GM and WM. Observational study of WM fiber tracts of two-sample subjects as the adjunct to current neuroimaging assessment is highly useful to reflect the value in differential diagnosis. Since TBSS is well-known for its whole brain voxel-wise analysis, it is incorporated as a statistical approach to discover the structural marker of atrophy between two groups of subjects, and relate the findings to the anatomical distribution of WM microstructural damage or the microstructure brain changes in cortical GM.

1.2 Problem Statement

The change of brain structural markers is the diagnostic feature for the most prevalent brain diseases. Developing a robust approach for early recognition of the disease at the prodromal stage is significantly required. At the mild cognitive impairment stage of the Alzheimer disease (AD), the valid diagnostic marker is the atrophy of medical temporal structure [33]. In temporal lobe epilepsy (TLE), the atrophy of the subcortical brain structures specifically the size of the hippocampus is observed [34]. Besides these neurodegenerative diseases, there is a significant evidence showing that the long-term 'Ketum' drug abuse also causes dementia which are profound impairments of learning and memory. These cognitive-impairing effects are revealed by the analysis of electroencephalogram (EEG) that shows a significant decline of delta power in the hippocampus [35]. Additionally, in the electrocorticography (ECoG) of the frontal cortex, it is found out that there is a complete suppression of the delta and theta bands [35]. Nevertheless, it is unclear whether there exists a potential biomarker of this drug addiction in the DWI neuroimaging evaluation. Even if there is an evidence that shows the location of biomarker that can relate the atrophy, it is unknown whether the cause of this atrophy is due to local degeneration of the nerve cells or caused by degeneration of the nerve connections or both. Hence, there is a need to develop analytics, visualization and workflow tools that can enable investigation on the effect of this drug addiction with the precise locations of the biomarkers in MRI imaging. There is also a need to identify suitable connectivity metrics that will inform on the quality of the nerve connection between sub-cortical brain regions that can correlate the cause of local degeneration of the nerve cells or degeneration of the nerve connections.

1.3 Objective

1. To provide a standardized protocol of WM tractography in reconstructing the 3D geometric and structural WM nerve fibers of the brain

2. To automate the process of segmentation of the WM fiber tracks of interest between the sub-cortical brain regions

3. To create an observational study of WM fiber tracts between the healthy subjects and the 'Ketum' drug addiction subjects for differential diagnosis

4. To develop an integral visualization of WM fiber tracts with the subcortical GM regions as the neuroimaging evaluation of finding the diagnostic biomarker in 'Ketum' drug addiction group

5. To be able in analyzing the atrophy of structural marker and relate to the anatomical distribution of WM microstructural damage or the microstructure brain changes in cortical GM

1.4 Scope of Study

- Methodology in obtaining the datasets of T1-w MRI and DT-MRI are understood and the preprocessing works on these datasets are explored.
- The subjects of "Ketum" drug addiction is investigated to study its effect related to the neurodegeneration of nerve fibers and nerve cells.
- Algorithms based on FSL and Dipy libraries are described to reconstruct the WM fiber tracts and the VTK library is utilized to create an analysis and visualization platform.
- The status of the WM fiber tracts of the "Ketum" subjects is examined for the length and magnitude for the whole brain and for the region of interest.
- Tract-Based Spatial Analysis (TBSS) is adopted to investigate the anatomical connectivity in the brains between the healthy and the "Ketum" groups.

2.0 LITERATURE REVIEW

2.1 Brain Structures and functions

The main organ of the human central nervous system is human brain. It is known as the command center to receive the information from the body sensors, interpret the information, and send the output to the body cells on how to response appropriately.

Human brain can be categorized into three main sections [23]. The first part is known as the forebrain, the second is the midbrain, and the third is the hindbrain. The forebrain has the cerebrum, thalamus, and hypothalamus. On the other hands, the midbrain comprises of the tectum and tegmentum. The hindbrain consists of cerebellum, pons, and medulla. Usually, we refer the midbrain, and the pons and the medulla from the hindbrain together as the brainstem.

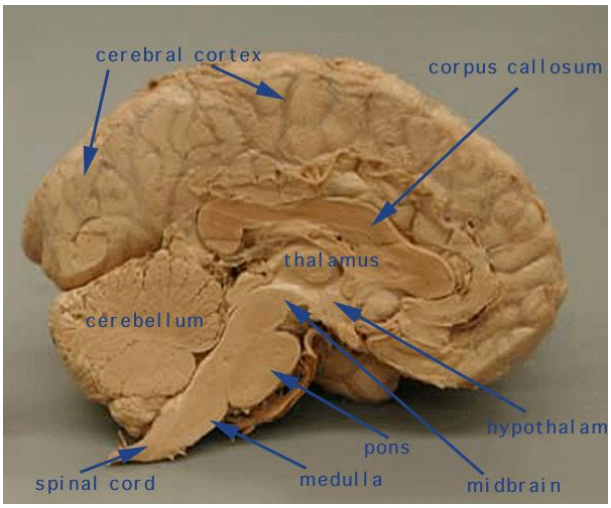

Figure 1 : Brain Structures [23]

The cerebrum, also cortex, is the biggest partition of the brain and the primary part of the forebrain. The cortex is involved in so many activities like thought and action. The cortex can be categorized into four lobes called the frontal lobe, the parietal lobe, the occipital lobe, and the temporal lobe [23]. The outer layer of the cortex, the cerebral cortex is highly folded to give a much larger surface area of the number of neurons in the confined volume. The cerebral cortex is made up of the gray matter. The gray matter comprises of mainly the cell bodies, unlike the white matter which is made up of the white myelinated sheaths of neural axons.

The cerebral cortex can be divided into two cortices, left and right cerebral hemispheres. Beneath the cerebral cortex is refered to as the subcortical structures. The subcortical regions includes the brainstem, cerebellum, hypothalamus, basal ganglia and so on. More detailed subcortical regions are illustrated in the Figure 2.

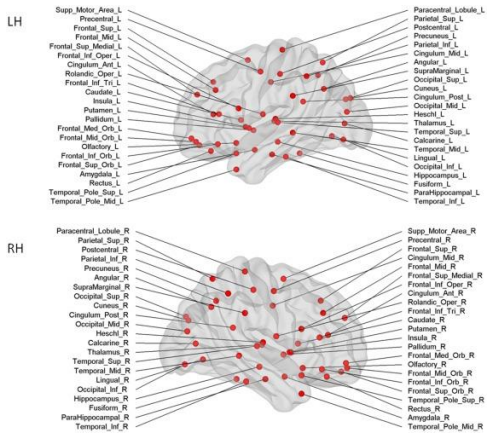

Figure 2: Cortical and Subcortical Regions [38]

To specifically describe the subcortical regions of the brain in imaging, the brain volume is normalized and segmented based on the location and intensity of the structures [39]. This is done by the FreeSurfer, a highly-automated brain image processing tool. By the segmentation, each voxel is automatically given by one of about 40 labels. These assigned labels are to differentiate different subcortical regions in the brain. which are Left-Cerebral-White-Matter (labeled as 2), Left-Cerebral-Cortex (labeled as 3), Left-Hippocampus (labeled as 17) etc [40]. The assignation of label (an integer value) in the subcortical brain regions allows different interested parts of the brain being segmented and studied in details of the brain neuroanatomy with the DTI data. A similar label found in the regions of the brain volume denotes the areas belong to the same region-of-interest.

2.2 Basic Neuron (Grey vs White)

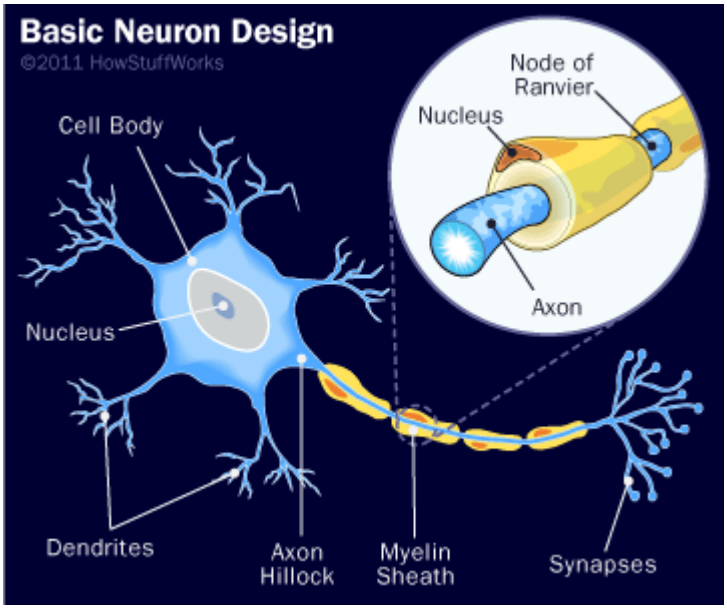

Figure 3 : Basic Neuron [8]

Together with the spinal cord, the brain makes up the central nervous system (CNS). The brain contains of approximate 100 billion of neurons (nerve cells) that are further categorized into the grey and white matter [8]. The neuron is what makes you clever, because the neuron is responsible to gather and transmit electrochemical signals, analogy to the gates and wires in the processor.

As shown in the Figure 3, typically, the neuron has a soma which is a cell body that has a cell nucleus, dendrites and a single axon [8]. To transmit the signal to other nerve cells, muscle cells and so on, achieved by electrochemical signal, the neuron transmits the pulses through the axon which is mostly covered by a layer of myelin sheath that can accelerate the transmission. For your information, there is only one axon in each of the neutron to transmit the signal from the cell body towards other neurons. The junction with which the two nerve cells make connection is called the synapses. The dendrites, appearing like the tree-like branching structure, is to collect information from other cells at synapses and relay the information into the soma.

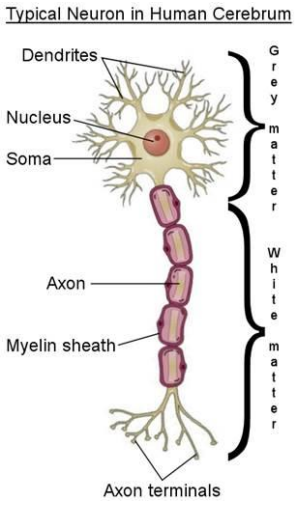

Figure 4 : White vs Grey Matter in Neuron [7]

To specify the white and the grey matter in the neutron [7], the dendrites, the synapses, the soma, and the nucleus make up the grey matter, whereas the axon and axons terminal build up the white matter, as shown in the Figure 4. The reasons of appearing in the grey-brown color are the grey matter containing the neuronal cell bodies and capillary blood vessels, and being relative to the lack of myelin. On the other hands, the white matter looks white because of the large amounts of myelin sheath which is a fatty protein that serves as the insulating and protective coating around the nerve fibers. In other words, the white matter is a neuron that have myelinated nerve fibers which is axon and does not have dendrites.

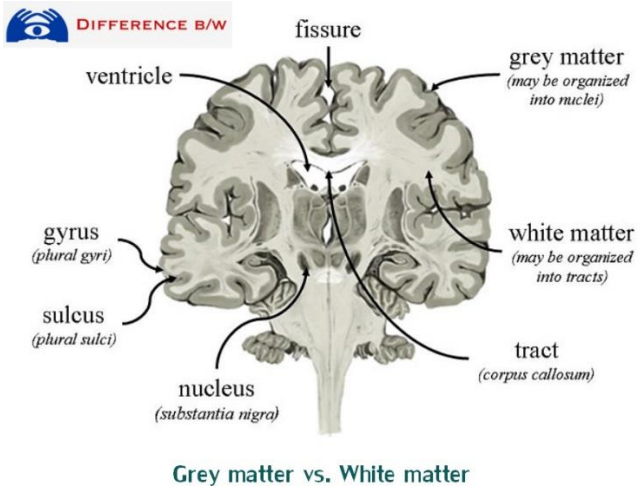

Figure 5 : White vs Grey Matter in Brain [20]

In fact, the grey matter has the most of the brain's neuronal cell bodies. At the surface of the cerebral and cerebellar cortices, it is where the grey matter can be found. Besides, in the depth of the cerebrum, cerebellar, brainstem, and spinal grey matter, there are also grey matter, as shown in the Figure 5. Hence, it can be concluded that the grey matter is involved in many regions of the brain that is related to muscle control and sensory perceptions such as memory, decision making, hearing, seeing, speech, and emotions [20].

Described as the bundles of axons, also called the fiber tracts, the white matter connects various gray matter areas in the brain. Apart from building up the large part of the deeper brain matter, the white matter also forms the superficial layers of spinal cord [16]. There are three different kind of fiber tracts that links one part of the brain to another part of the brain and to the spinal cord, as shown in the Figure 6 and Figure 7.

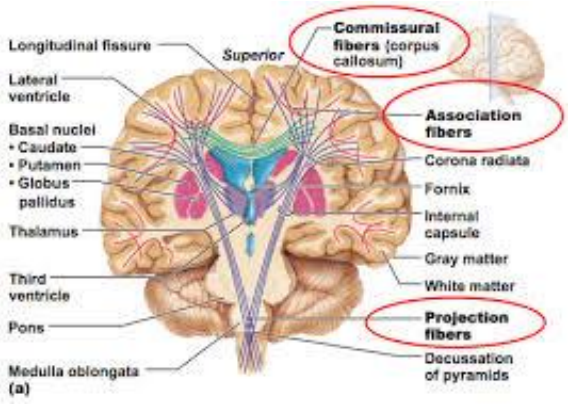

Figure 6: Fiber Tracts in Brain [62]

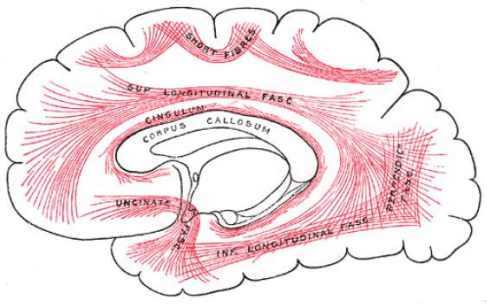

Figure 7: Different Association Fiber Tracts [61]

- Commissural fibers: Connecting two hemispheres (left and right) of the brain
- Association fibers: Connecting cortical lobes within the same hemisphere of the brain
- Projection fibers: Connecting cortex to other parts of the brain or to the spinal cord

2.3 Diffusion Weighted Imaging (DWI)

Magnetic resonant imaging (MRI) is a scan that utilizes a powerful of magnet field and radio waves to form pictures of body organs and structures [11]. The digital images form the MRI scan are very useful to diagnose a variety of conditions of diseases. Unlike computerized tomography (CT) scan, the MRI scan is a non-ionizing radiation imaging modality to create informative diagnostic images.

The main advantage of MRI scan is it creates multiple imaging contrast for different kinds of tissues. The different types of MRI contrast are created by the different sets of MRI protocols. To acquire these MRI images, multiple MRI pulse sequences are created, which are the different programed sets of changing magnetic fields executed in a series of commands by the computer software. There are numbers of parameters in each MRI pulse sequence [9]. These various MRI pulse sequences set by different parameters are grouped together into an MRI protocol, designed to specifically access different parts of human body [5].

A popular form of MRI protocol, diffusion weighted imaging (DWI) constructs according the measurement of the random Brownian motion of water molecules per a voxel of tissues [15]. Diffusion-weighted imaging (DWI) are the conventional MRI sequences that are widely utilized by clinicians as the generally preferred neuroimaging examination based on the gray-white brain tissue contrast [2,4]. It includes T1-weighted (T1W) gadolinium (Gd) enhanced and spin-echo T2-weighted imaging (T2W) scans.

By measuring the water molecules with diffusion-weighted MR pulse sequence, the mean diffusion within a voxel can be expressed as a 3-D diffusion tensor [10]. If the water molecules diffusion is found to be isotropic, the tensor will appear in a sphere. If the water molecules diffusion is found to be anisotropic, the tensor will appear in an ellipse.

However, this motion described by the DWI is confined by the membranous membrane. Hence, diffusion tensor imaging (DTI) is the extension of DWI [6] that permits the data profiling according the white matter tract orientation. This is because along the white matter tract, the water diffusion flows along the pathway of least resistance, which builds up the final image consisting of the directions of maximum water diffusivity along the

fiber tracts. This final image is the 3D visualization of neuronal pathways giving the white matter information.

2.4 Diffusion Tensor Imaging (DTI)

The diffusion tension imaging (DTI), being the new MRI technique, is to outline the axonal organization of the human brain. Since the image contrast in MRI is based on the signals from the proton which comes from the water molecules in our body, the DTI signals is controlled by the water protons. Hence, based on the physical properties of water molecules in our body, we can generate the MR contrast from the following simplified Equation 1 [18],

$$S = PD\left(1 - e - \frac{TR}{T_1}\right)e - \frac{TE}{T_2 e} - bD$$

Equation 1

Where,

- S is MR signal (S) in a spin-echo image
- PD is proton density, representing water concentration
- T1 and T2 is relaxation times, representing signal decay after time excitation
- D is Diffusion Coefficients, representing Brownian motion of water molecules
- TR is timing of excitation (repetition time)
- TE is the preparation period (echo time)
- b is the diffusion weighting factor

It is important to note that the S magnitude that is obtained from the MR scanners is to delineate the physical properties of water molecules. On the other hands, the TR,TE, and b-factors are the control variables that are used to change the weighting (T1,T2,D) to the signal. Making the TE and TR times short, T1W image is produced with the contrast and brightness are predominately determined by T1 properties of tissues. In contrast, by making the time of TE and TR long, the T2W image is produced. To differentiate between T1W and T2W images, CSF is the best to be distinguished because of it appears dark in T1W image but bright in T2 image [42].

However, this equation is not enough to depict the diffusion orientation from a single intensity value, S in T1W and T2W images. Hence, we require the additional parameter, so-called the diffusion coefficients, D to denote the diffusion orientation.

To retrieve the diffusion orientation from the diffusion coefficients, D, it can be done by using the different b-factors in the Equation 1, and meanwhile keeping the other imaging parameters constant, such as TR and TE. To illustrate it clearly, let the b-factors as b1 and b2 in two experiments [18, 24]:

$$Experiment\ 1 : S_1 = PD\left(1 - e^{-TR/T_1}\right)e^{-TE/T_2}e^{-b_1 D}$$

$$= S_0 e^{-b_1 D}$$

$$Experiment\ 2 : S_2 = S_0 e^{-b_2 D}$$

$$\frac{S_2}{S_1} = e^{-(b_2 - b_1)D}$$

$$D = -\ln\left(\frac{S_2}{S_1}\right)/(b_2 - b_1)$$

Equation 2

Where,

- S0 (MR signal at baseline) is the constant derived from PD,TR,TE
- S1, S2 is the signal after the diffusion gradients have been applied

Hence, the signal intensity differences can be used to find the diffusion coefficients, D. On the other hands, b-factor is a value that is derived from the strength, duration, and spacing of the gradient pulses or gradient.

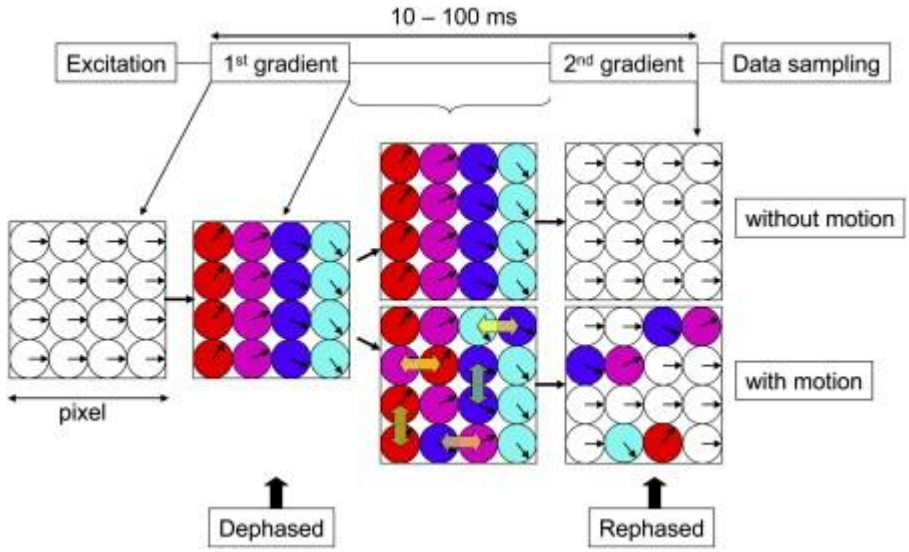

Figure 8: Gradient Pulses [18]

A schematic diagram above shows how the application of (X, Y, Z) gradient units illustrate the water motion in a pixel. Assume the gradient is applied at the horizontal orientation. Seeing each circle symbolizing water molecules at different locations, the vectors in each circle indicate the respective phases of the signal. After the first gradient pulse is finished to introduce a phase, the second gradient pulse is applied at 10 - 100ms after, to rewind the phase that has been introduced. If there is a movement of water molecules between two gradient applications, the rephrasing would fail at the application of second gradient, resulting the signal phase dispersion along the x-axis. This imperfect refocusing results the signal loss. Hence, this phase difference can be used to detect the water diffusion.

By increasing the gradient amplitude and duration, a larger b-factor can be achieved to generate the stronger diffusion effects, yet the more signal loss we expect, because of the longer the interval between the gradient pulses allows more time for water to move around, resulting more signal loss [3] and [13]. In other words, consider the water molecules in a pixel, there higher the rate of water molecules diffusion, the more de-phased the water molecules are. Hence, there will be weaker the recorded S signal.

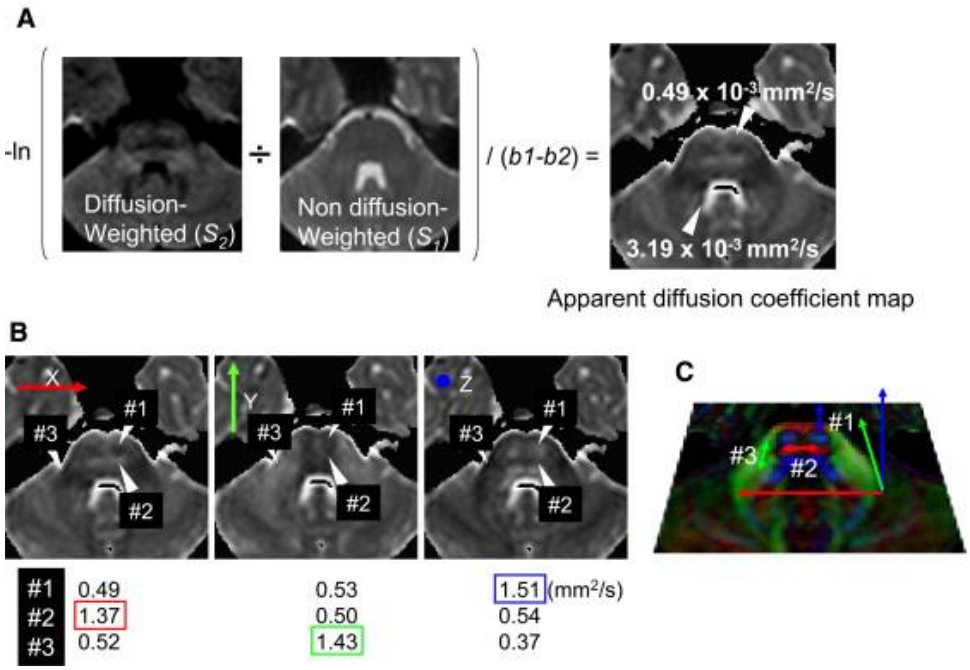

Figure 9: Color-coded Orientation Map [18]

Now, solving the equation (2) at each pixel, a map of the D can be calculated for the overall picture as shown above Figure 9A, where the X gradient is only concerned. So, this is how the apparent diffusion coefficient (ADC) map is introduced along the X-axis. Seeing the ADC map, one can conclude that the intensity (mm2/s) of each pixel is proportional to the extent of diffusion. Combining the X, Y, Z gradients, the ADC along any X, Y, Z gradients is measurable, shown in the Figure 9B. To determine the orientation or color for each pixel based on the largest ADC, the red, blue, green colors are assigned into the respective X, Y, and Z axes. As a result, a color-coded orientation map [22] is formed shown in the Figure 9C to determine the water molecules along the axonal fibers. Put it another way, the largest ADC indicated by the color boxes illustrate the fiber orientation [17], yet the lower of the intensity signal in the DWI [19].

Practically, to figure out the orientation with the largest ADC, there are thousands of axes to be measured, which become impossible to be implemented, because the fiber orientation is not always along or oblique to the X, Y, Z axes. Thanks to the concept of diffusion tensor introduced in early of 1990s [4]. The measurements along different axes can be good enough represented in a 3D ellipsoid which contain three eigenvalues, λ_1, λ_2,

and λ_3 and three eigenvectors, $\mathbf{v}_1$, $\mathbf{v}_2$, and $\mathbf{v}_3$, defined by 6 parameters that are obtained at each pixel, and represented in 3x3 symmetric matrix [14].

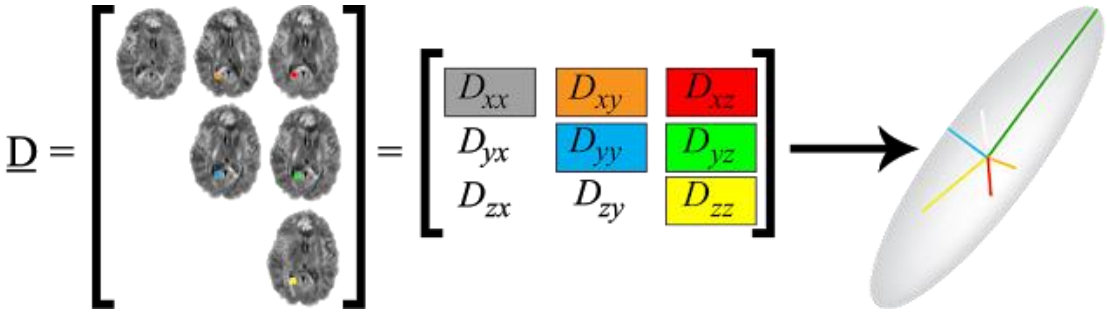

Figure 10: Diffusion Tensor [18]

Seeing the Figure 10, it can be summarized that the diffusion tensor for a single voxel can be obtained by imaging the diffusion in the six different gradient directions. Similarly, the other voxels in the entire MRI scan is being applied with the similar approach. From the diffusion tensor, the magnitude, the orientation of directional diffusion and the extent of anisotropy can be represented numerically [1], and it is expressed in the symmetric 3x3 matrix in the diffusion ellipsoid [12].

2.5 T1W neuroimaging analysis

T1W image best describes the brain structures and it is the most basic pulse sequence in MRI. Depending on the types of tissues, the signal appearing in the T1W image is different, from dark to bright. The dark region seen on the T1W image is mainly because of the tissues that have fast-flowing blood, whereas the bright region is owing to the fat, hydrogen-containing structures and slow-flowing blood. In other words, WM is bright and GM is dark in the T1W image.

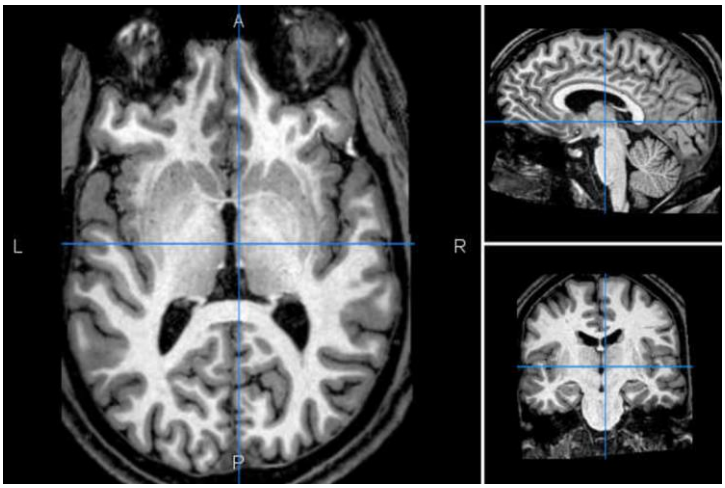

Figure 11 : T1-weighted MRI scan [42]

T1W images exhibits the gray-white brain tissue contrast. The bright regions are the WM, whereas the grey regions are the GM. Meanwhile, CSF appears as the dark regions.

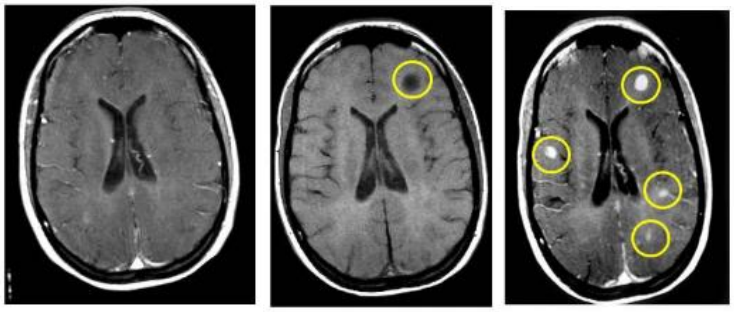

Figure 12 : T1-weighted MRI with lesions [43]

The unusual brighter and darker spots appear on the above T1W images is the marker of the lesions [43]. The lesions can be the result of the atrophy due to the neurodegenerative diseases.

2.6 DTI neuroimaging analysis

The rate of water diffusion in brain along the tissues is different because of the type, architecture, integrity and presence of barriers [44]. Measuring the water diffusion quantifies the shape of the tensors in each voxel. Fractional Anisotropy (FA) is the most widely used measure. The FA represents the fraction of the tensor that indicates the extent of aligned structures. Ranging the FA value from zero to one, the isotropic water diffusion is assigned to zero, whereas the higher FA value denotes the increased directionality of diffusion, regardless of the rate of diffusion [45]. Despite of the FA is the DTI summary measure that is adequate for a board spectrum of pathological conditions, the FA alone is not enough to describe the full tensor shape [46].

To demonstrate more specific information on the WM pathology, the axial diffusivity (AD), the radial diffusivity (RD), and the mean diffusivity (MD) are the quantitative methods besides the FA. Since MD is the mean of three eigenvalues within a voxel, it reflects the rate of water diffusion per voxel, regardless the directionality [45]. On the other hands, the RD constructs from the rate of water diffusion in the transverse direction per voxel, and the AD maps from the diffusion rate along the main axis of diffusion [44]. A recent developed measure, Geodesic Anisotropy (GA) is based on the distance of a diffusion tensor to the closet isotropic tensor [48]. The equations [47] of tensor quantification are shown below.

$$\lambda_{1=} longitudinal\ (axial) diffusivity (AD)$$

Equation 3

$$\frac{(\lambda_2 + \lambda_3)}{2} = radial\ diffusivity\ (RD)$$

Equation 4

$$\sqrt{\frac{1}{2}} \frac{\sqrt{(\lambda_1 - \lambda_2)^2 + (\lambda_1 - \lambda_3)^2 + (\lambda_2 - \lambda_3)^2}}{\sqrt{(\lambda_1^2 + \lambda_2^2 + \lambda_3^2)}} = fractional\ anisotropy\ (FA)$$

Equation 5

$$\left(\sum_{i=1}^{3} \log_2 \lambda_i / \langle D \rangle \right)^{1/2} = Geodesic\ anisotropy, where\ \langle D \rangle = det(D)^{1/3}$$

Equation 6

2.7 Fiber Tracking and Tractography

Deterministic and Probabilistic fiber tracking are two important algorithms of white matter tractography to track the trajectories of fiber bundles. Depending on the purposes, one can work better than the other in linking and mapping the intervoxel connectivity based on the pattern of the anisotropic diffusion tensor of water flowing in the axonal directions [28].

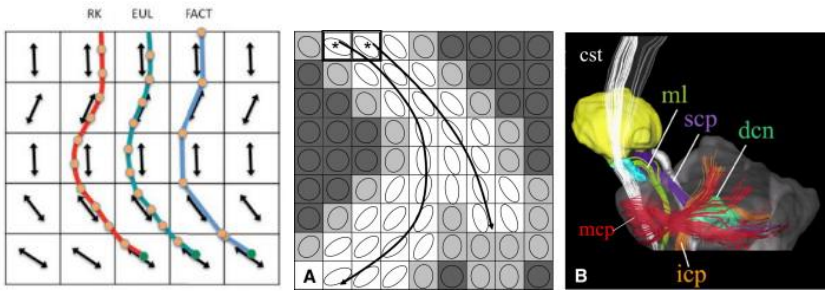

Figure 13: Tractography Algorithms and 3D Tract Reconstruction [31, 18]

The deterministic tractography algorithm maps out the white matter anatomical connections based upon the major eigenvector of the diffusion tensor from voxel to voxel in 3 dimensions. In fact, it can be done in three different kinds of fiber integration methods. First, Fiber Assignment by Continuous Tracking, known as FACT, is performed in linear step-wise integration methods, and alters the direction of streamline at every edge of voxel [31]. Similar to FACT, Euler method is done in linear step-wise integration methods. However, the fiber trajectory changes its direction at every fixed step size. On the other hands, Runge-Katta methods is a non-linear stepwise and high-order integration to give a smooth, more linear and more accurate solution to curved trajectories.

Unlike the deterministic fiber tracking, the probabilistic fiber tracking includes the expected uncertainty into the algorithm by modelling the propagation direction as a probability density function on the principal diffusion direction to produce a connectivity metric for each voxel. These uncertainties in diffusion direction can be due to the probability of the co-existence of multiple fiber-crossing in a voxel, subject motion and image noise. By using the local probability distribution, the probability fiber tracking can identify multiple possible routes for a trajectory for the connection with any other voxel.

In fact, the probability fiber tracking can disperse more trajectories in lower SNR [30], especially in the case of crossing fibers.

Regardless the probabilistic or the deterministic algorithms, both have their own pros and cons to reconstruct the 3D WM structures of the entire brain in research studies [25].

2.8 Fiber Segmentation and Clustering

Analyzing overall streamlines of around 1 million tracts in a human brain to study for his specific anatomical information is an impractical way. Therefore, WM segmentation is a critical step in measuring and visualizing the only-interested-streamlines that pass through a region-of-interest (ROI). The ROIs are the cortical and subcortical regions that have been assigned with labels early using Freesurfer tool. For example, the label of 2 indicates the region of Left-Cerebral-WM, the label of 41 indicates the region of Right Cerebral White Matter. By superposing the ROIs with the WM streamlines, the tracts that traverse through the ROIs are extracted. These tracts are called the bundles of interest (BOIs) [27]. The BOIs includes the left/right unicinate fasiculus, left/right longitudinal fasciculus, corpus callosum etc. By analyzing the BOI alone, any loss of axonal tracts can be the sign of a biomarker for assessing the WM abnormalities.

To further reduce the level of WM tractography datasets in neuroimaging interpretation, clustering is incorporated to group a set of streamlines in such a way they are related to the nearby tracts. This approach in forming the clusters are based on the position, shape, and distance [27]. A cluster centroid is highlighted from the cluster to represent the average of all tracts in the cluster. Clustering is crucial to statistical data analysis, including data compression, pattern recognition, machine learning, image analysis etc [50].

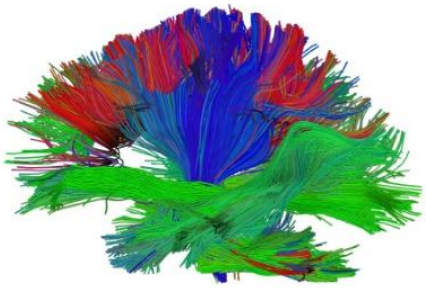

Figure 14: WM Streamlines [49]

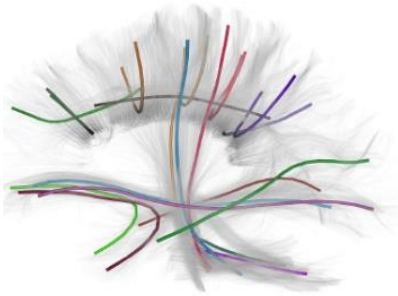

Figure 15: Clustered Streamlines [49]

Figure 16: Segmented Streamlines [49]

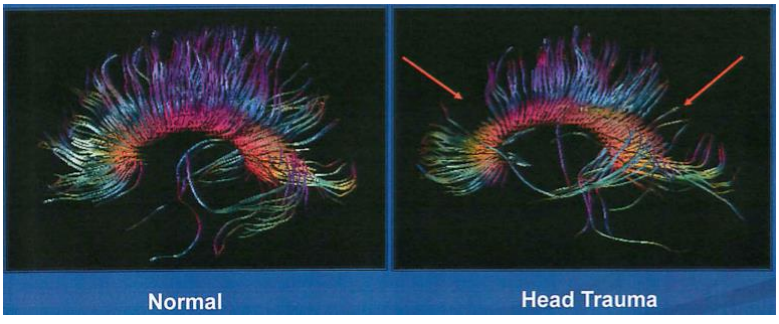

Figure 17: Loss of WM indicating Head Trauma [60]

2.9 Tract-Based Spatial Statistics (TBSS)

Tract-Based Spatial Statistics (TBSS) is famous for its whole brain voxel-wise analysis for a group of diffusion tensor Fractional Anisotropy (FA) images. It is an approach that analyzes and compares the DTI subjects statistically by aligning the FA images from multiple subjects [52,53,54,55]. The result of the TBSS that suggests the global decrease of FA is a strong neuroimaging biomarker to investigate the WM changes between two groups of subjects [56].

The aim of this study is to investigate and compare the WM structures of a control group of healthy subjects with a group of 'Ketum' drug addiction subjects. To run the TBSS, the standard FSL TBSS pipeline [51] is used and specified as the Figure 18.

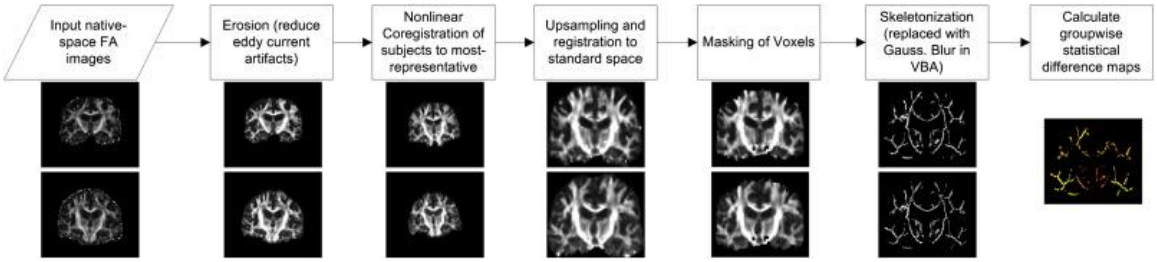

Figure 18: TBSS pipeline [51]

The step of TBSS starts with the eddy current correction to eliminate the unusual bright spots in the FA images, because of the eddy current-induced distortions in CSF voxels. Next, nonlinear registration is performed to register all the images into the most representative subject. After that, the co-registered images are upsampled to the MNI standard space. Masking of voxels which only includes the nonzero voxels in the images is then performed. As the final step of TBSS before running the voxelwise cross-subject stats, skeletonization is carried out to generate the FA skeleton mask. With the 4D skeletonized FA image, the groupwise statistical difference maps is performed to observe any change of WM structure between two groups.

3.0 METHODOLOGY

3.1 Project Activities

Project title selection and allocation	• Project title "**Software Tool for Brain Connectivity Analysis**"
Literature review and background study	• Study brain structures, neuron structures, DWI, DTI, Segmentation and Clustering Algorithm
Data Acquisition	• 14 DTI datasets provided by USM used to study the effect of 'Ketum' drug addiction related to the dementia
Data Pre-processing	• Understand the necessary of BET, MCFLIRT, Eddy_correct to MRI images
WM Tractography	• Study DIPY for WM tractography • Compare tractography algorithm with DSI-Studio
WM Segmentation and Clustering	• Compare the result of auto and manual WM segmentation algorithms • Study Quickbundles Clstering to WM
GUI Development	• Develop 3D-Observational Platform taking T1W image with WM streamlines • Develop 3D-Differential tool comparing two sets of WM streamlines
Fiber Intrepretation and Analysis	• Analyze the length of WM streamlines • Analyze the magnitude of WM streamlines
Streamline Metrics and Analysis	• Relate the WM streamlines to the cortical and subcortical regions
Tract Based Spatial Statistics	• Compare the anatomical connectivity between the healthy and the 'Ketum' drug addiction group using FA tensor models

3.2 Gantt Chart

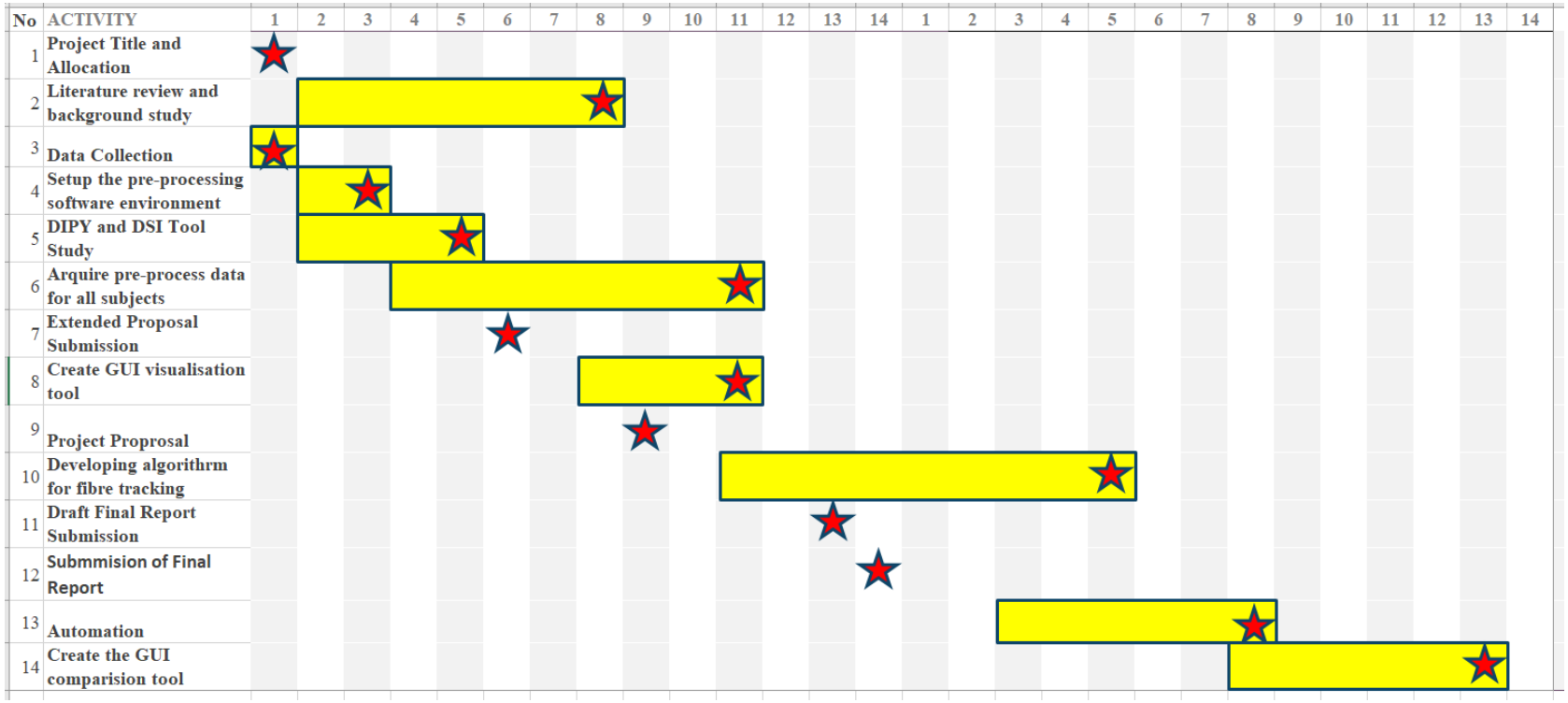

3.3 Data Acquisition

Diffusion Tensor Imaging (DTI) datasets from two groups of subjects were acquired from Universiti Sains Malaysia (USM) to study the effect of 'Ketum' drug addiction related to early neurodegenerative symptoms. The images from the first group were provided by 7 healthy subjects, and the following images of the latter were obtained from the 7 Ketum users. The degree of diffusion weighting (b-value) was 1000 s/mm2. Three non-diffusion sensitization (b=0) images were acquired in earliest of the MRI scan, following by the 30 different directions of diffusion weighting. For fiber tracking, the files of b0, DTI, bval, bves, aparc+aseg are only needed and located in one database folder.

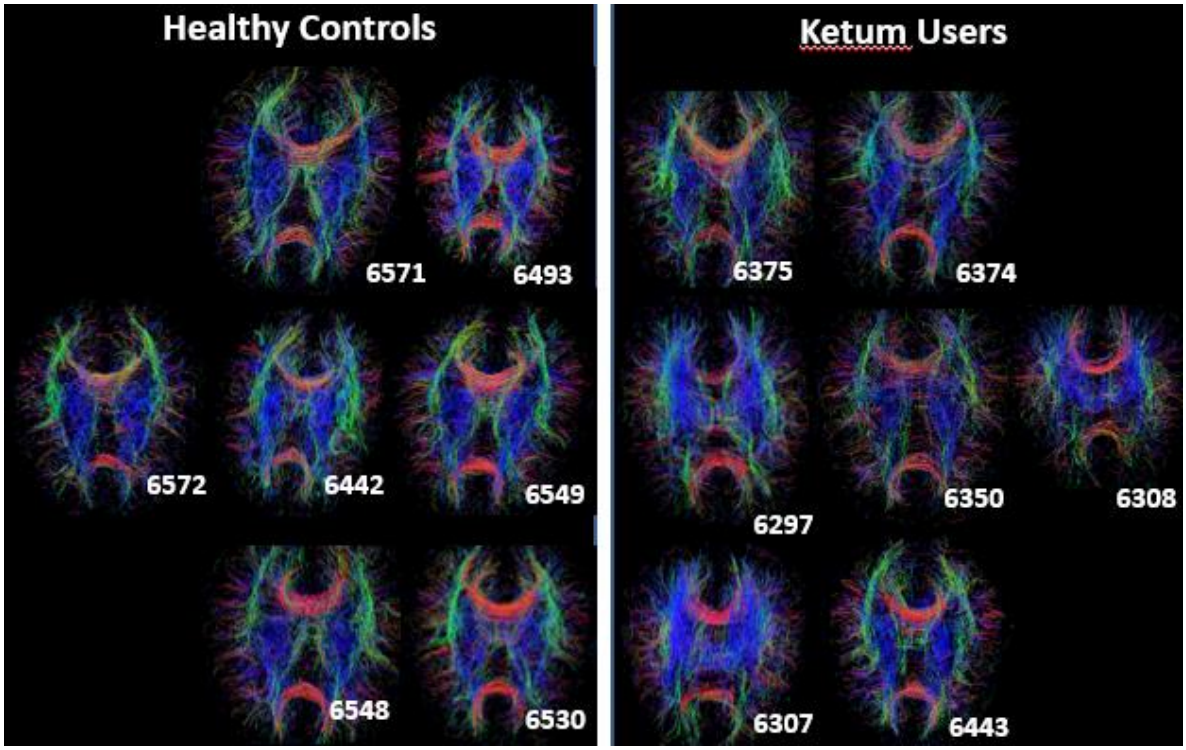

Figure 19: Healthy and Ketum User Subjects [59]

3.4 Image Preprocessing

Before working on the DTI datasets, the Brain Extraction Tool (BET) is applied on each of the subjects used to eliminate the non-brain issues which are mostly the external skull surface in MRI images. Motion artifacts pose a serious problem in accurately characterizing the size, shape, and tissue properties of brain structures [57]. MCFLIRT, the developed tool by FSL, is utilized to perform the motion correction on every T1W image to avoid any effect of motion artifacts and guarantee the voxel-wise correspondence. To DTI images, eddy current correction (eddy_correct by FSL) is required as a significant step of pre-processing. This is to avoid the distortions such as false fiber tracking, image intensity loss, and enhanced background in the subsequent steps of image processing [58].

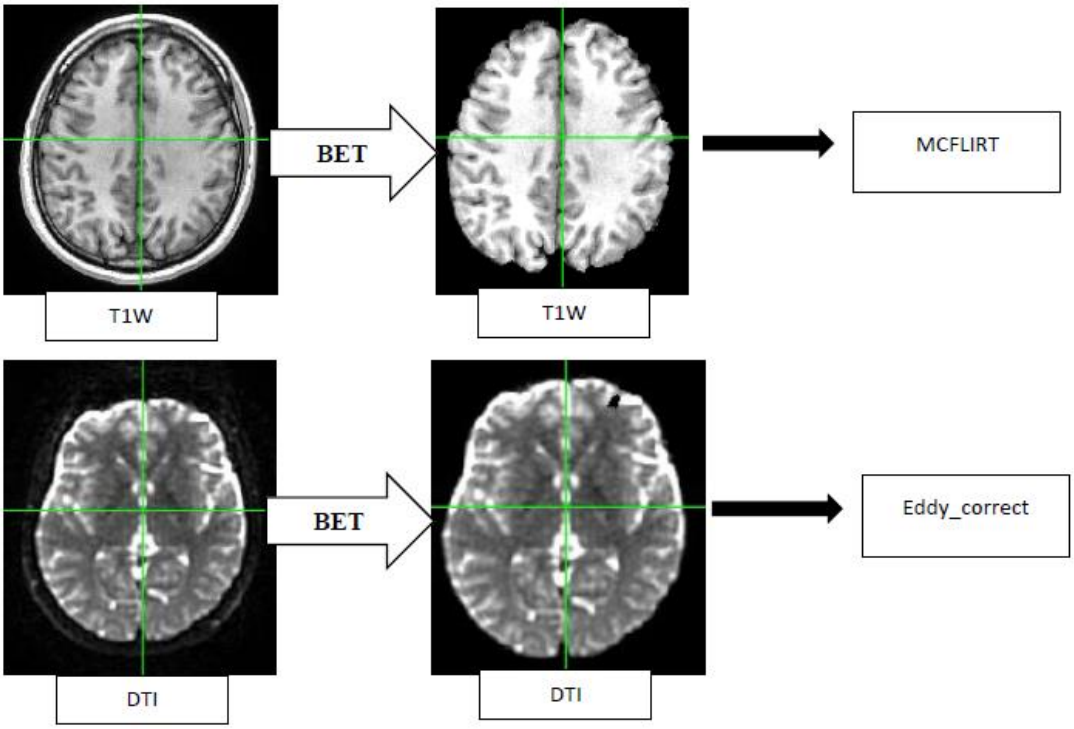

Figure 20: T1W and DTI Pre-processed Data

3.5 Image Processing

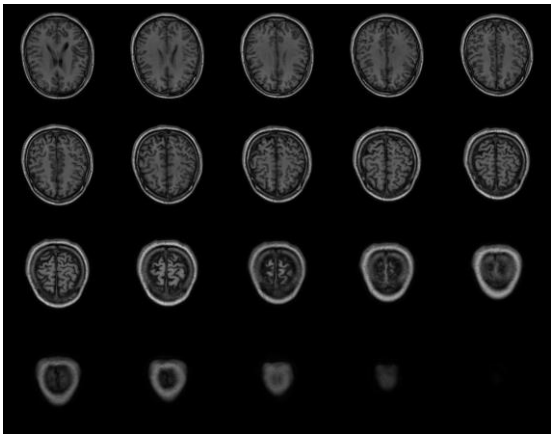

Figure 21: Brain Transverse Slices of '6297' Subject

Given the T1W medical image data, the brain volume of the subject is segmented into slices using 'SimpleITK' library. For example, the transverse image of the subject from slices 15^{th} to 35^{th} are segmented for the study of brain matter, soft-tissues, and anatomical structures.

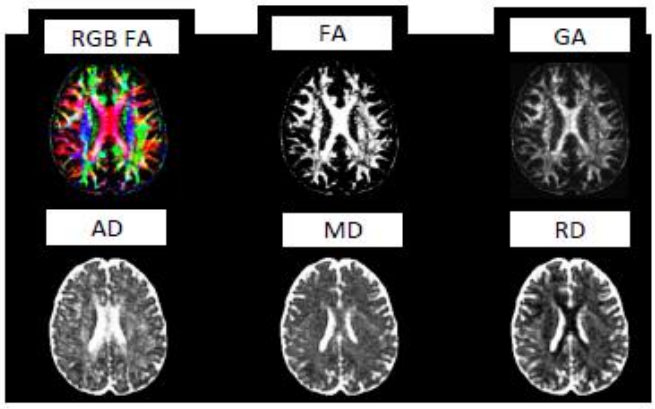

Figure 22: Diffusion Tensor Models of Subject '6297'

The scalar maps of different diffusivity measures in quantification of the local tensors are generated with the developed algorithm of Dipy library. The fractional anisotropy (FA) with RGB color, fractional anisotropy (FA), geodesic anisotropy (GA), axial diffusivity(AD), mean diffusivity (MD), and radial diffusivity (RD) are generated for each of the subjects. To show the tissues contrast among them, a simple interface is created to plot each slice of the scalar maps, which is useful to analyze the conditions of brain tissues described in every tensor model.

3.6 Fiber Tractography

Euler Delta Crossings (EuDX) from the dipy library [49] is employed as the deterministic tracking algorithm to reconstruct the streamlines. To begin with, the input parameter of seeds is initiated to 8 seeds per voxel to grow the streamlines. The propagation step size is specified as 0.5 for the Euler integration. To terminate, the parameter of tensor FA with threshold 0.05 is set as the stopping criteria. To resolve multiple intravoxel fiber orientations in the MR images, Constant Solid Angle ODF (Q-Ball) is used as the reconstruction model in EuDx with the Spherical harmonics order (SH) set to 6.

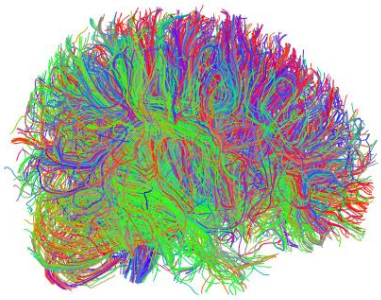

Figure 23: WM Tracts in Sagittal Slice

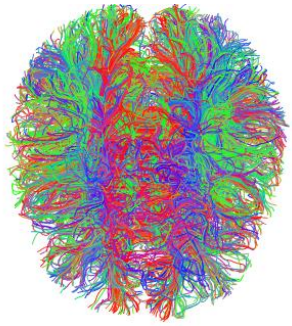

Figure 24: WM Tracts in Transverse Slice

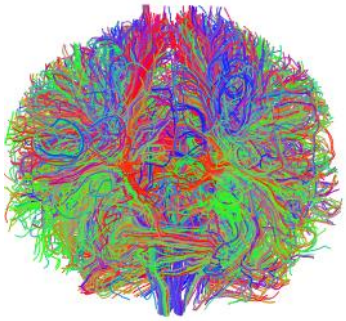

Figure 25: WM Tracts in Coronal Slice

The WM tracks coming in different shapes, lengths, and positions, has been reconstructed throughout the brain using the deterministic tractography. As shown in the Figures 23, 24 and 25, the WM tracts that belongs to the subject '6297' is presented and color-coded in RGB. The local orientation of the fiber tracks is indicated in the combinations of RGB colors, where the red indicates a latero-lateral direction (left-right), the green indicates an anterior-posterior (front-back) direction and the blue indicates the dorsal-ventral (upper-lower) direction, and the intermediate orientations is indicated with the other colors.

3.7 Fiber Segmentation

To compare the fiber bundles among the subjects, segmentation is processed to filter the fiber bundles of interest from the whole WM tracts for specific analysis. The whole WM tracts is first registered in the MNI standard space using FSL Linear Image Registration Tool (FLIRT) and then non-linear transformation using FSL Linear Image Registration Tool (FNIRT). This is to ensure every subject has the common space for analysis and interpretation. Next, the single-subject template called the WMPM TYPE II Eve Atlas (a 32-year old healthy female) that contains the manual parcellation of 130 ROIs is used to segment the fiber bundles. The result is saved in 'trk' file format. To demonstrate the streamlines, the 'trk' files is read as the input and rendered in the VTK interface, as shown in Figures 26, 27, 28, 29 and 30.

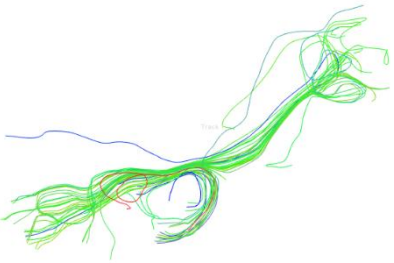

Figure 26: Left Uncinate Fasciculus

Figure 27: Corpus Callosum

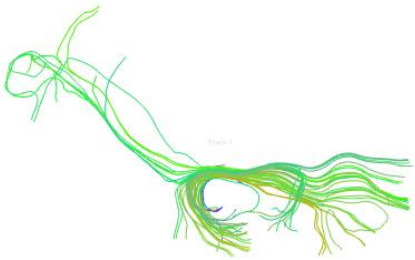

Figure 28: Right Uncinate Fasciculus

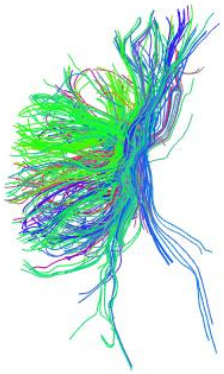

Figure 29: Left Superior Longitudinal Fasciculus

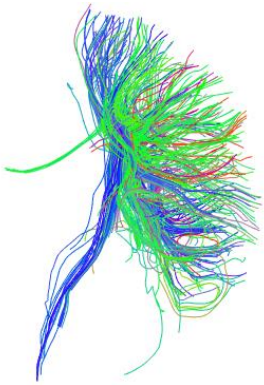

Figure 30: Right Superior Longitudinal Fasciculus

3.8 Fiber Clustering

Having all streamlines of the brain generated in densely packed, the clustering algorithm called Quick-Bundles (QB) in Dipy library is implemented to ease the interpretation. By implementing the QB algorithm, the tracks are down-sampled to 12 points without making changes to the length, and 10 mm distance threshold that determines the cluster size. The clusters' centroids of the streamlines of every subject are generated, followed by the streamlines are color-coded with the corresponding centroids' colors. To demonstrate the result, the Vtk library is utilized to create a rendering window to show every cluster of the streamlines and the pertinent clusters' centroids.

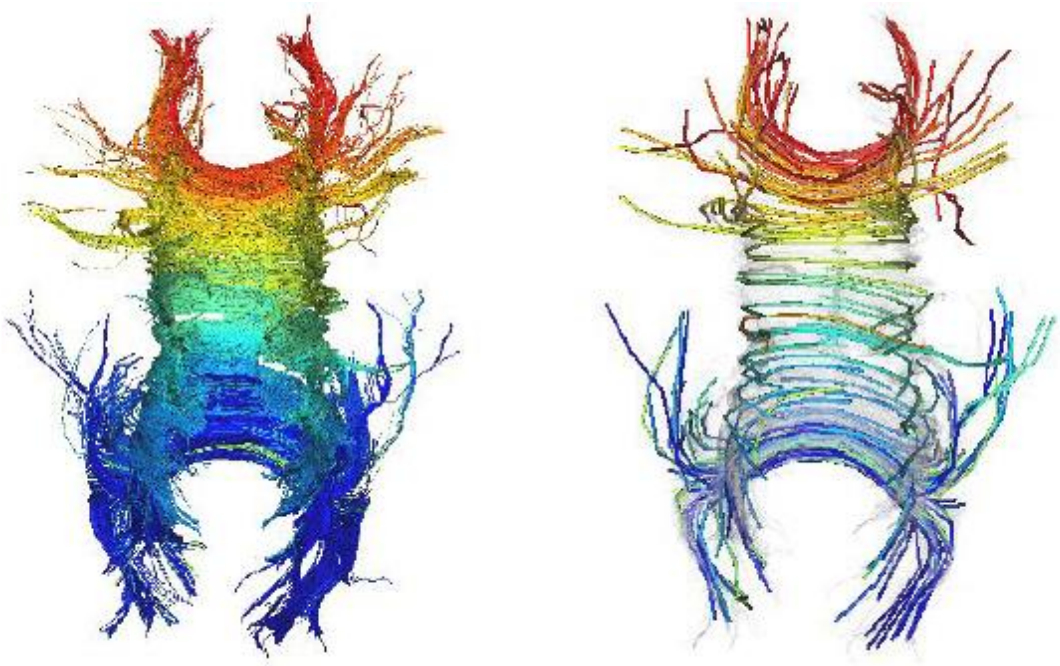

Figure 31:(Left) Segmented corpus callosum; (Right) Centroids after Clustering

3.9 Graphical User Interface (GUI)

To summarize all the processing steps, it is illustrated in the flow chart below. A Graphical User Interface (GUI) is developed for being an easy-to-use tool to automate the complicated processing steps in reconstruction of the 3D WM structures and analysis.

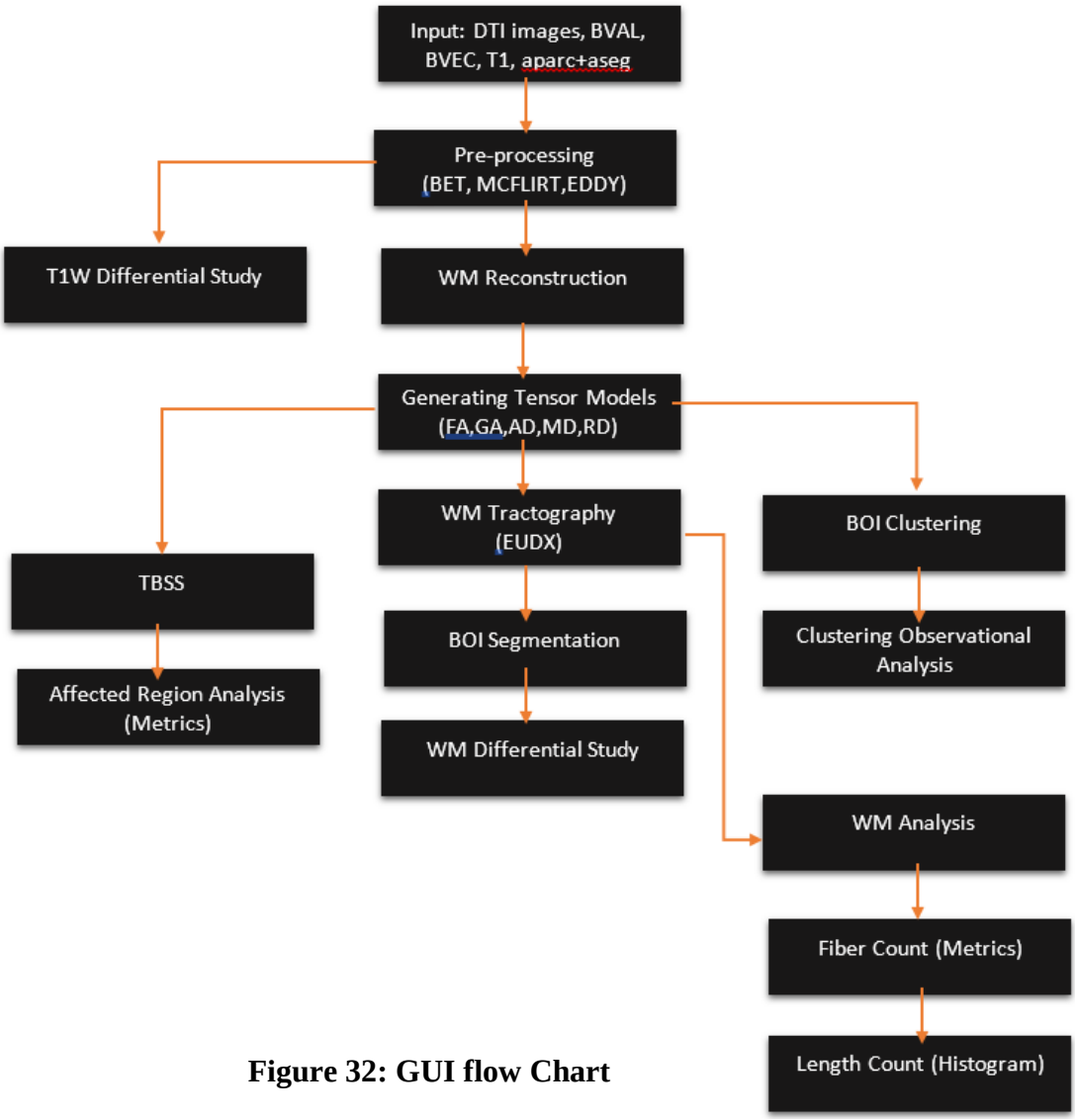

Figure 32: GUI flow Chart

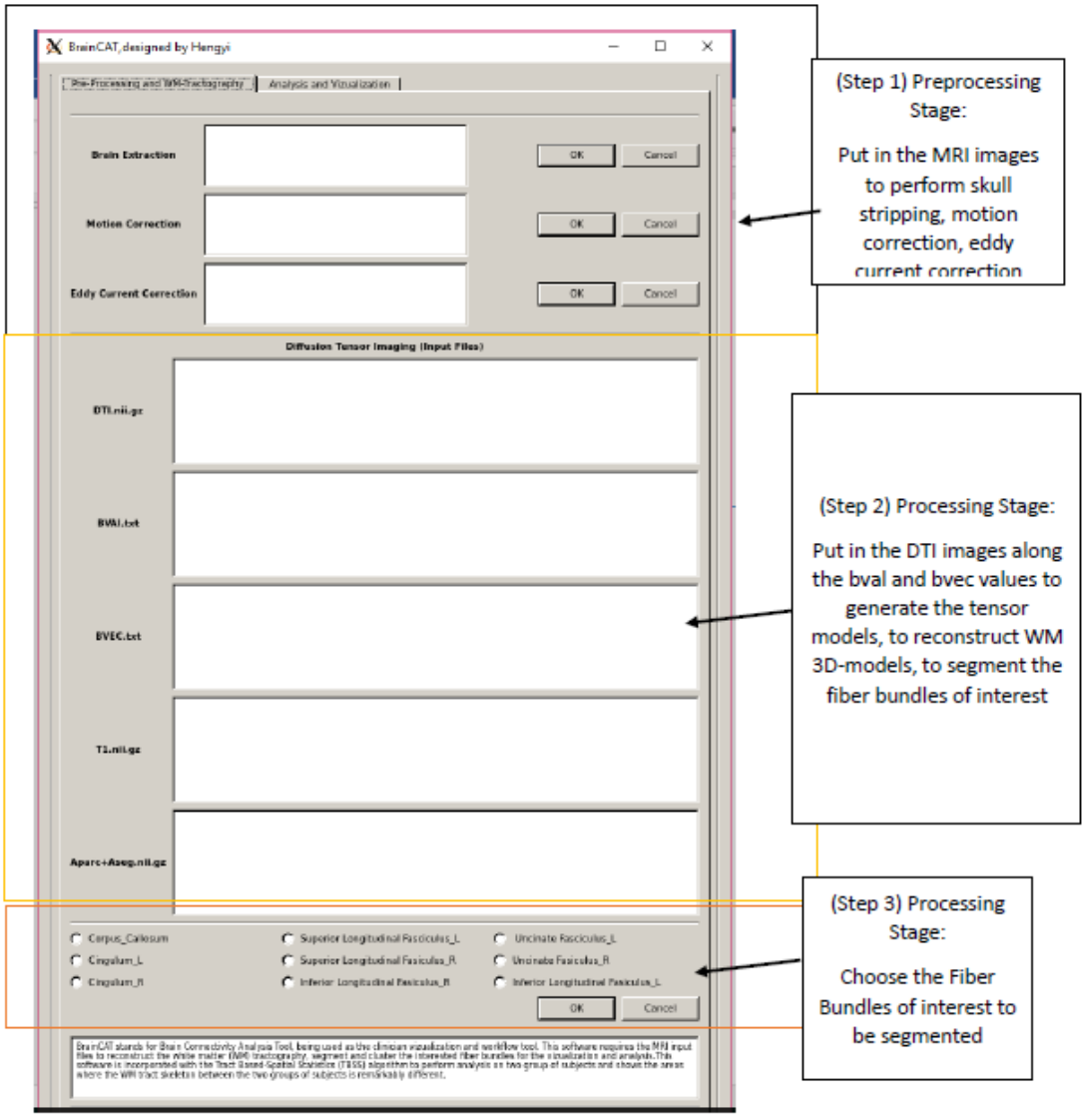

Figure 33: GUI (Part 1)

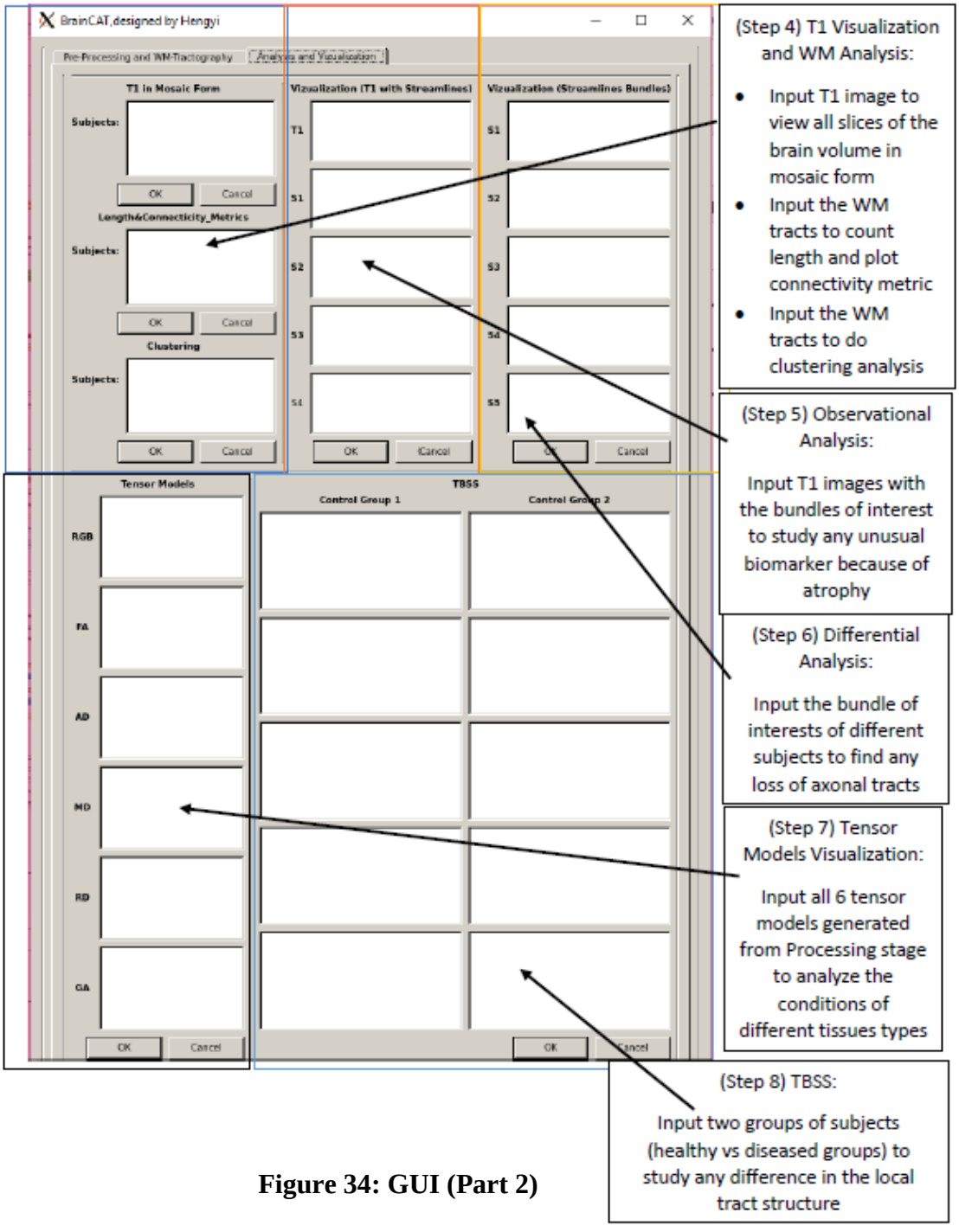

Figure 34: GUI (Part 2)

4.0 RESULT AND DISCUSSION

4.1 T1W Images Differential Analysis

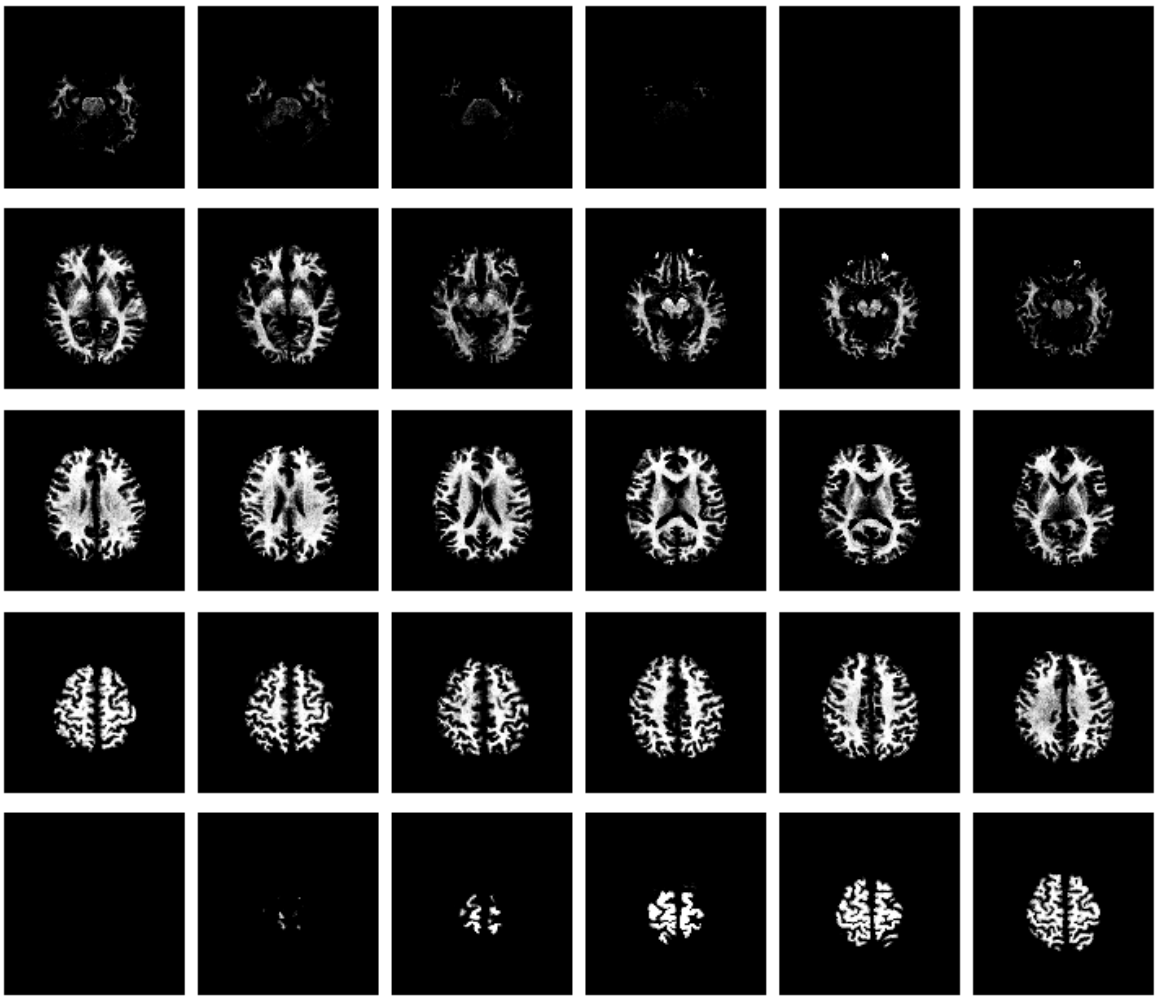

Figure 35: Transverse Slices of Subject '6297'

To improve the visualization interface of studying the T1W datasets of a single subject, a renderer is created with Dipy library to quick segment and demonstrate all slices of either the transverse, sagittal or coronal images. As shown in the Figures 35, the transverse slices of the '6297' subject brain volume is rendered. Features like pressing 'Shift' at the meanwhile scrolling the mouse enables the images to be zoom in and zoom out. Pressing 'Shift' at the meanwhile moving the mouse enables the specific image dragged to focused in camera view. Similar to the coronal and sagittal view of the T1W image of subject '6297', the slices of the brain volume are demonstrated.

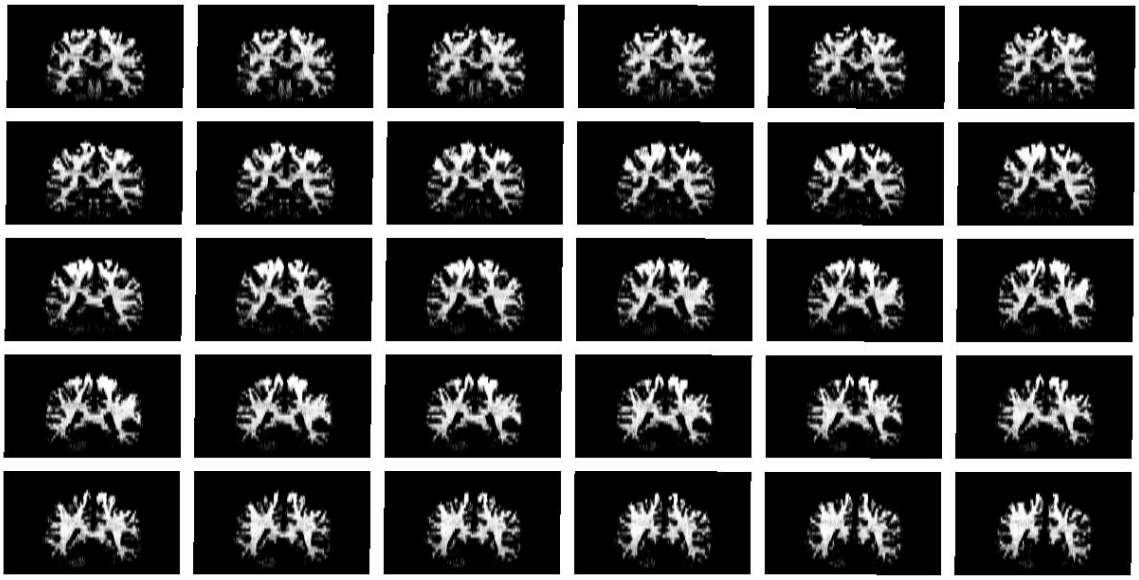

Figure 36: Coronal Slices of Subject '6297'

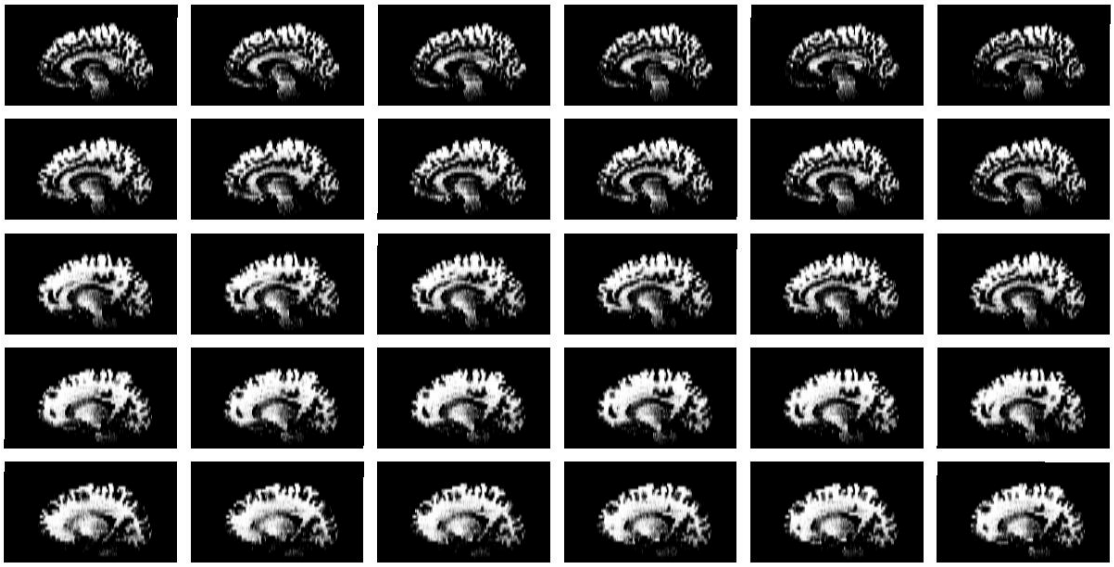

Figure 37: Sagittal Slices of Subject '6297'

As the grey-white contrast depicted in the Figures 35, 36 and 37, the white brain tissues are bright, while the neurons appear dark-grey, and the CSF is black. By analyzing the T1W images across every subject of the healthy and the 'Ketum' group, one at a time, there is no unusual brighter and darker spots found.

To ease the differential analysis in T1W image, an interface of viewing and comparing the similar axial, coronal, and sagittal slices of different subjects is significantly required. It allows the clinicians to interpret any usual difference in structures among the subjects

of study. As seen in the Figures 38, 39, and 40, the sagittal slices of two groups of subjects are plotted for the differential study. The first row of the figures is the healthy subjects of 6571,6493,6572,6442,6549,6548,6530, whereas the second row is the ‘Ketum’ drug addiction subjects of 6375,6374,6297,6350,6308,6307,6443.

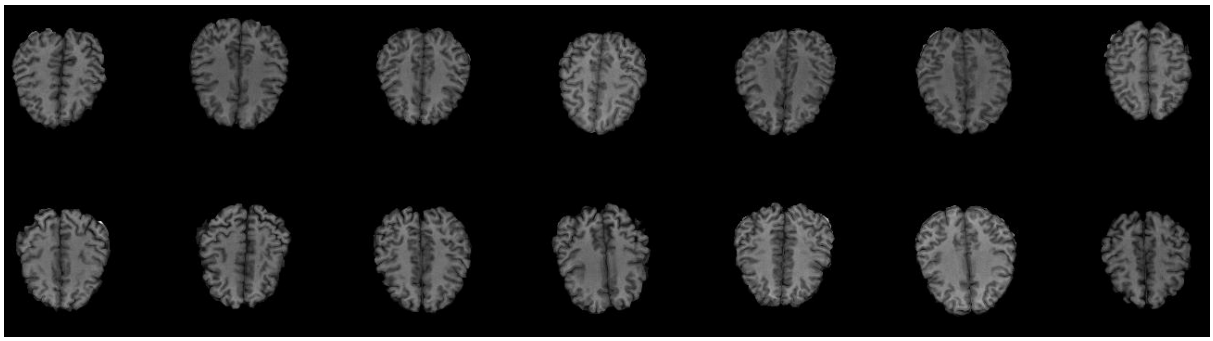

Figure 38: Transverse Slices of All Subjects of Study

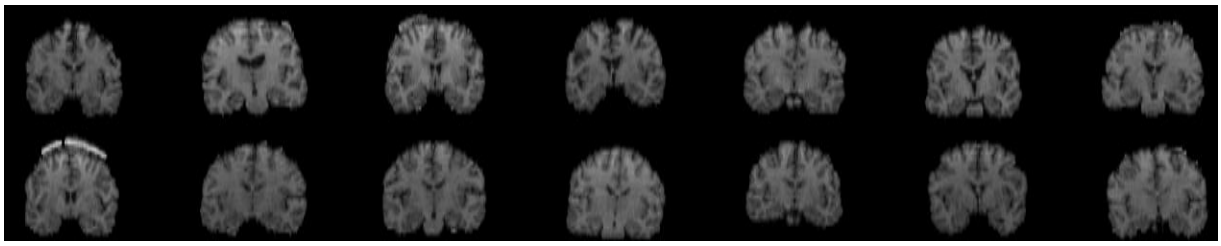

Figure 39: Coronal Slices of All Subjects of Study

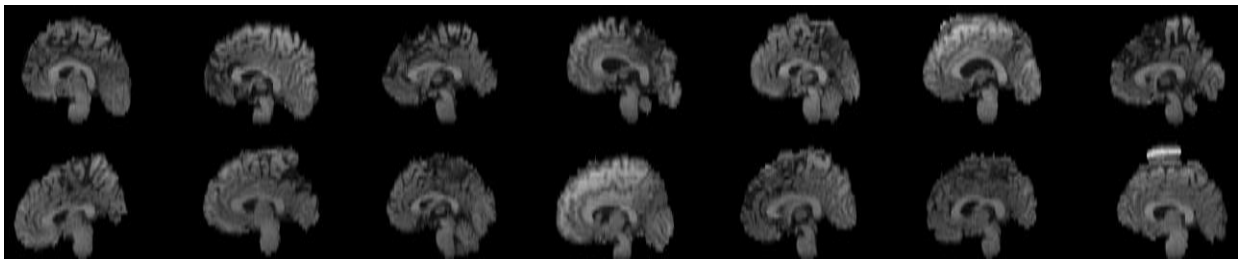

Figure 40: Sagittal Slices of All Subjects of Study

4.2 DTI Tensor Models Interpretation

Six tensor models are constructed based on five diffusion tensor measures of Fractional Anisotropy (FA), Geodesic Anisotropy (GA), Axial Diffusivity (AD), Mean Diffusivity (MD) and Radial Diffusivity (RD). They are RGB FA image, FA image, GA image, AD image, MD image, and RD image, and are generated for all the subjects of study. To demonstrate and meanwhile analyze the results of each subject, a visualization interface is created to show the tissue contrast of these images. Except for the color-coded RGB FA map, the grey-white contrast of the five following images indicates the presence of certain brain tissues.

Based on the reconstructed DTI scalars of the subject '6297', its biological microstructure especially the WM and GM exhibits in different grey-white contrast across the tensor models, except the RGB FA.

- Looking at the RGB Fractional Anisotropy (FA) map, the microstructural integrity of WM is color-coded based on the fiber orientation. The X, Y, and Z axes of the map are color-assigned with red, blue, green, indicating the particular strong directional the local tract is.
- Looking at the Fractional Anisotropy (FA) map, that depicts only grey-white contrast on the brain tissues, the microstructural integrity of WM appears bright and the GM appears dark, useful to study any damage in local tract structure
- Looking at the Geodesic Anisotropy (GA) map, that also depicts grey-white contrast on the brain tissues, the microstructural integrity of WM appears light-grey and the GM appears grey, also useful to study any damage in brain fiber microstructures
- Looking at the Axial Diffusivity (AD) map, the apparent bright side of the images indicates the changes of White Matter and its pathology, and it correlates to WM maturation.
- Looking at the Mean Diffusivity (MD) map, it is apparent that the bright side of the image indicates the cerebral spinal fluid (CSF), and useful to study axonal degeneration.

- Looking at the Radial Diffusivity (RD) map, the apparent bright side of the images indicates the presence of White Matter, and useful to study the WM demyelination.

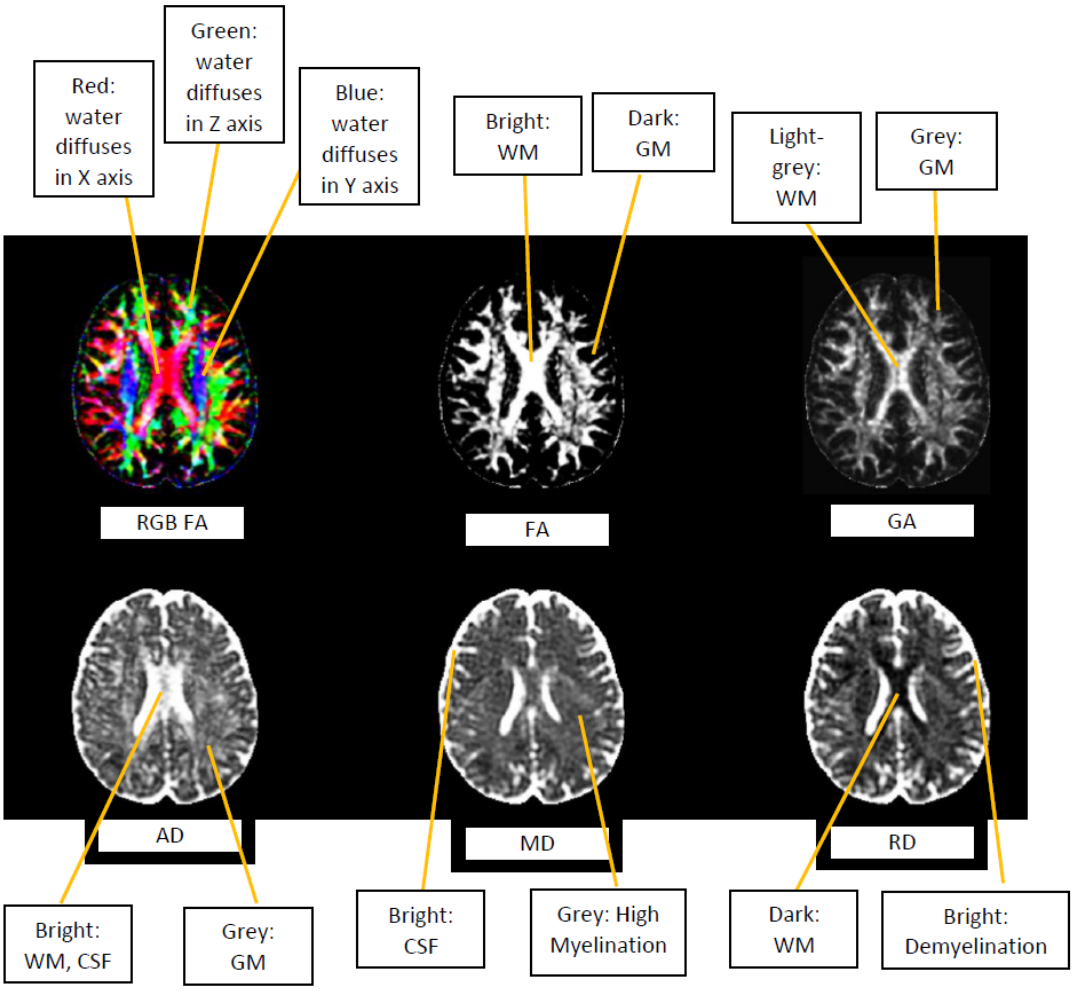

Figure 41: RGB FA, FA, GA, AD, MD, RD Tensor Models for Subject '6297'

4.3 Fiber Bundles Observational Study

Analyzing the T1W image alone is not enough to harness much of the information regarding to the structures of WM and GM. Hence, an integral visualization incorporated of the T1W image with the bundle of interest (BOI) is developed for the purpose of enhancing the biomarker potential. To demonstrate the usefulness of this interface, the corpus callosum of subject '6548' is segmented as the BOI and superimposed with its T1W image. The result is rendered in the visualization interface, and shown in the Figures 42 to 46.

Besides rotating, zooming in and zooming out of the view of the T1W image with the BOI, there are additional features developed in the interface and controlled by the sliders and buttons. The sliders of 'Moving-X', 'Moving-Y', and 'Moving-Z' is to move the BOI to superimpose the T1W image. This is because the initial position of the BOI is not overlapped nicely with the T1W image. On the other hands, the sliders of 'Axial', 'Coronal', and 'Sagittal' is to control the view of T1W image slice. The buttons of '+' and '-' are to control the opacity of the streamlines so that it provides a condition for clinicians to only analyze the T1W image.

With this interface, any unusual darker or brighter spot appears on the T1W image can be related to any loss of axonal tracts in the WM structures.

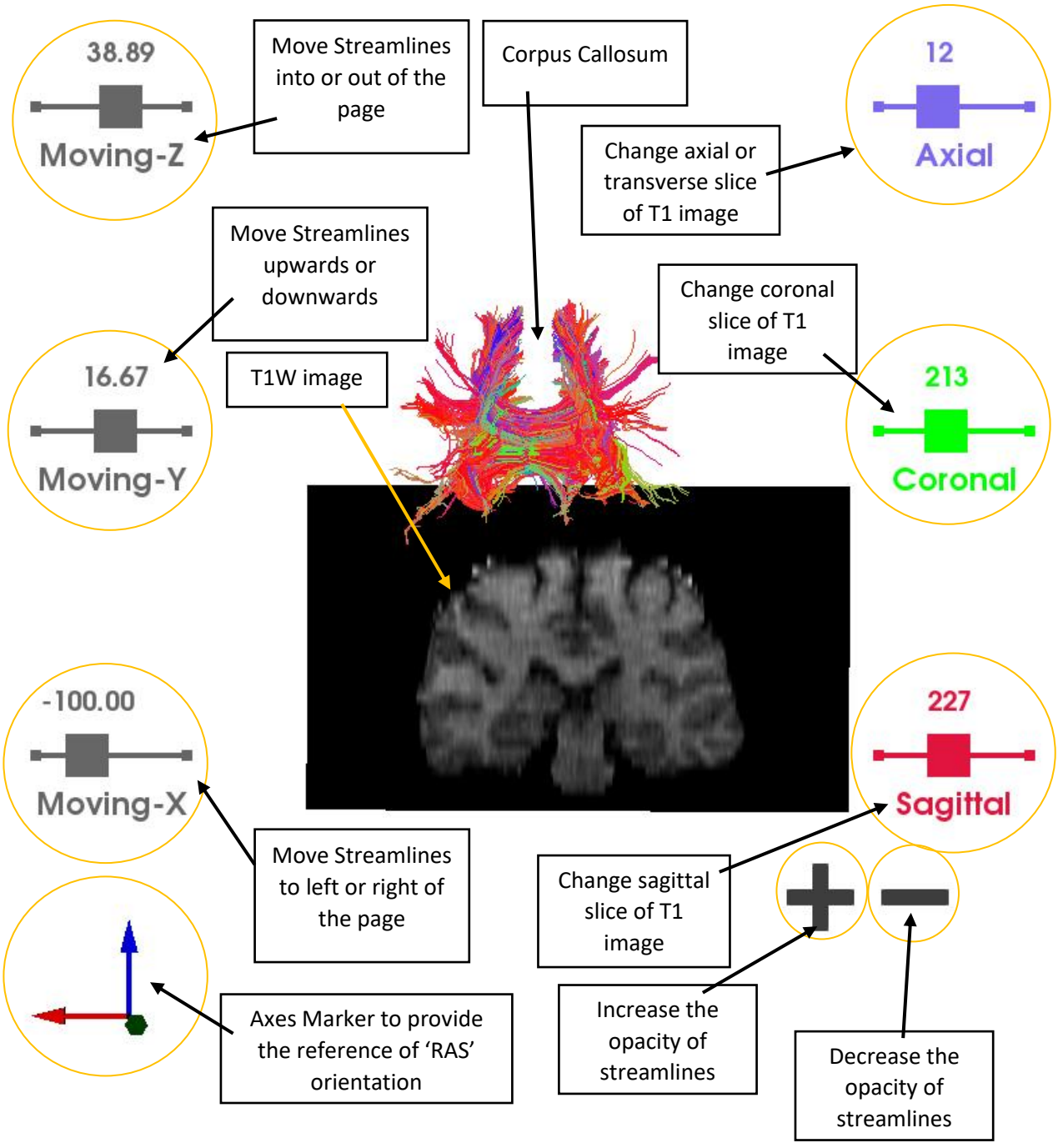

Figure 42: Integral Visualization tool (Part 1)

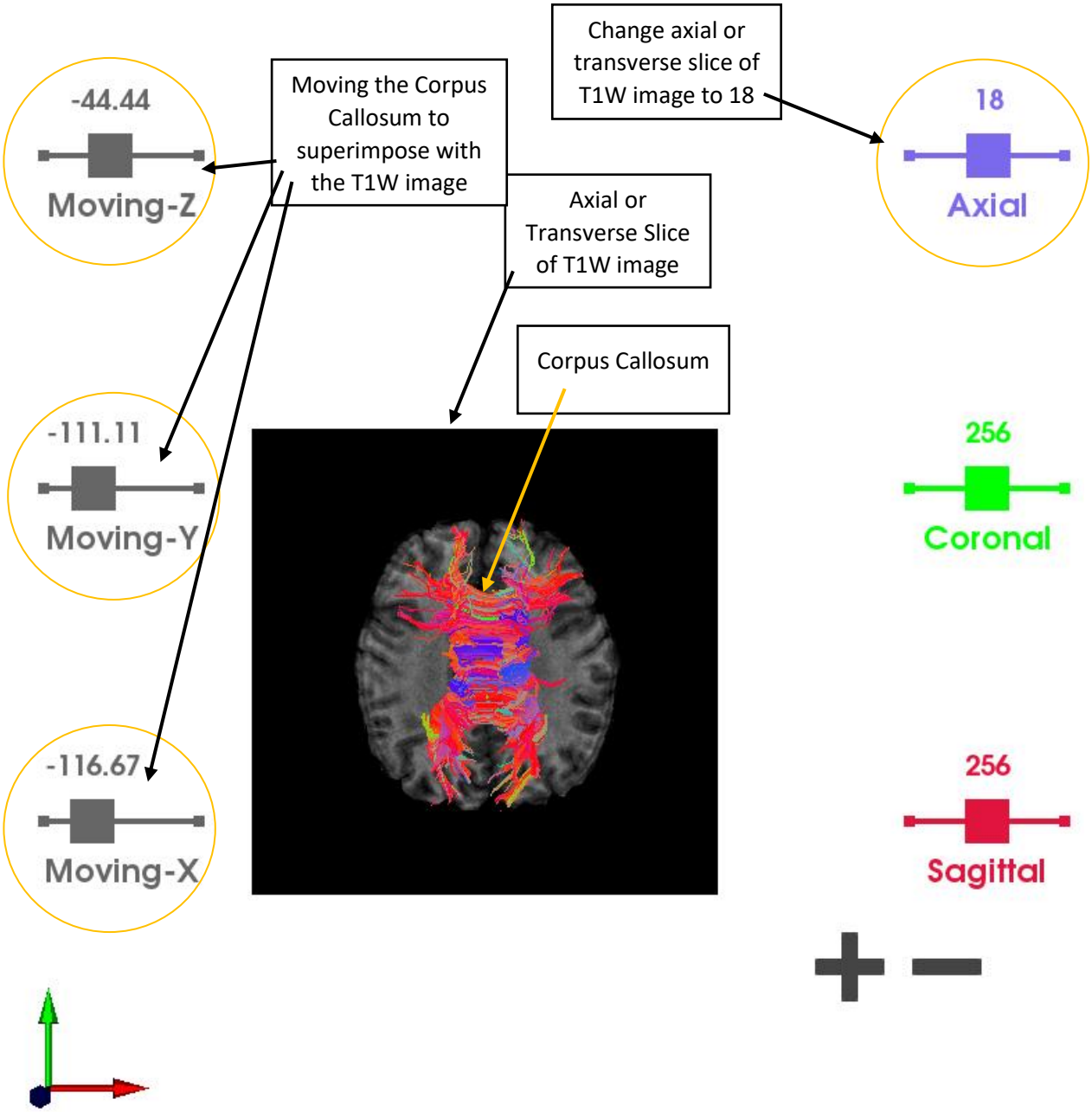

Figure 43: Integral Visualization Tool (Part 2)

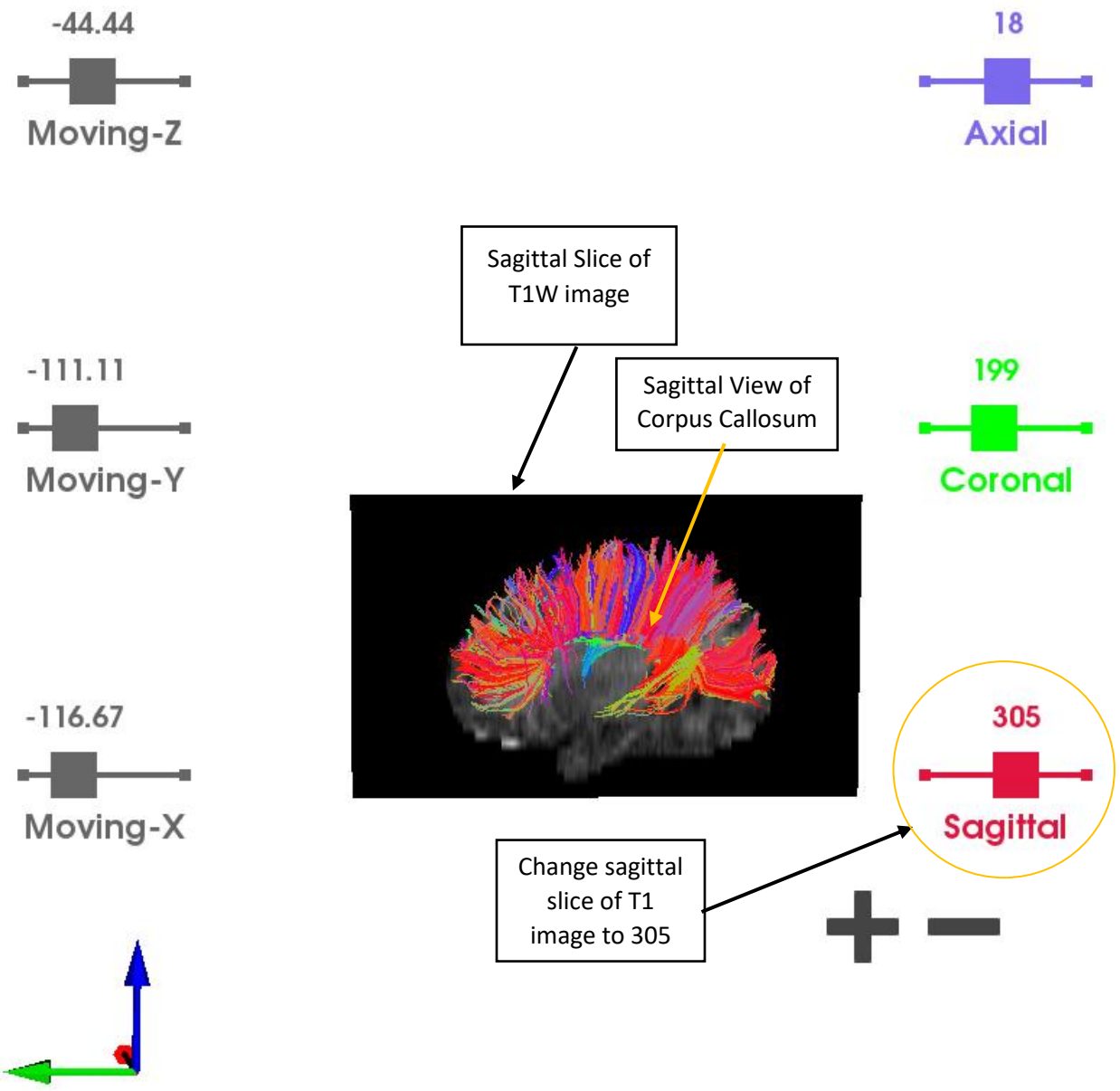

Figure 44: Integral Visualization Tool (Part 3)

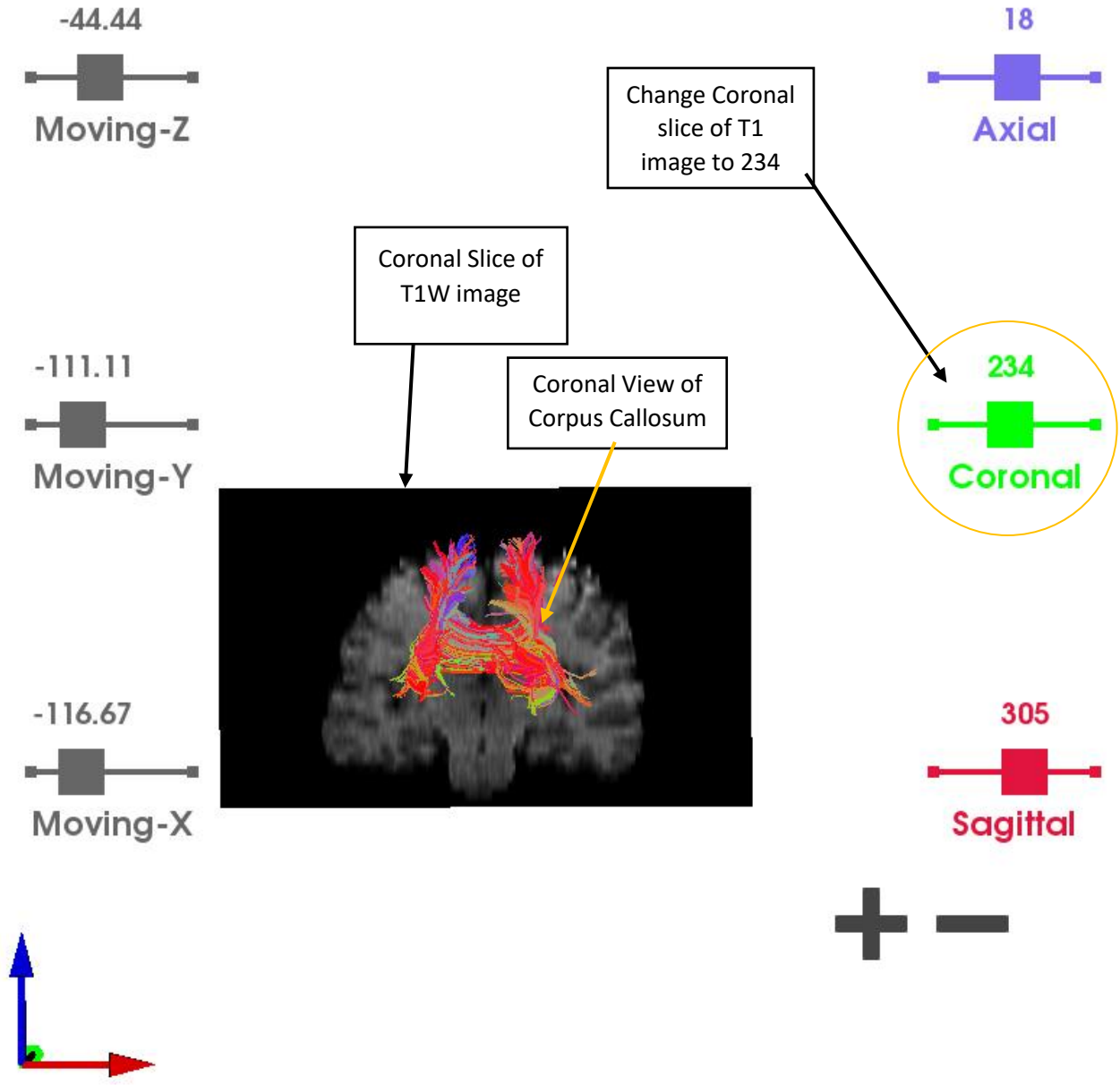

Figure 45: Integral Visualization Tool (Part 4)

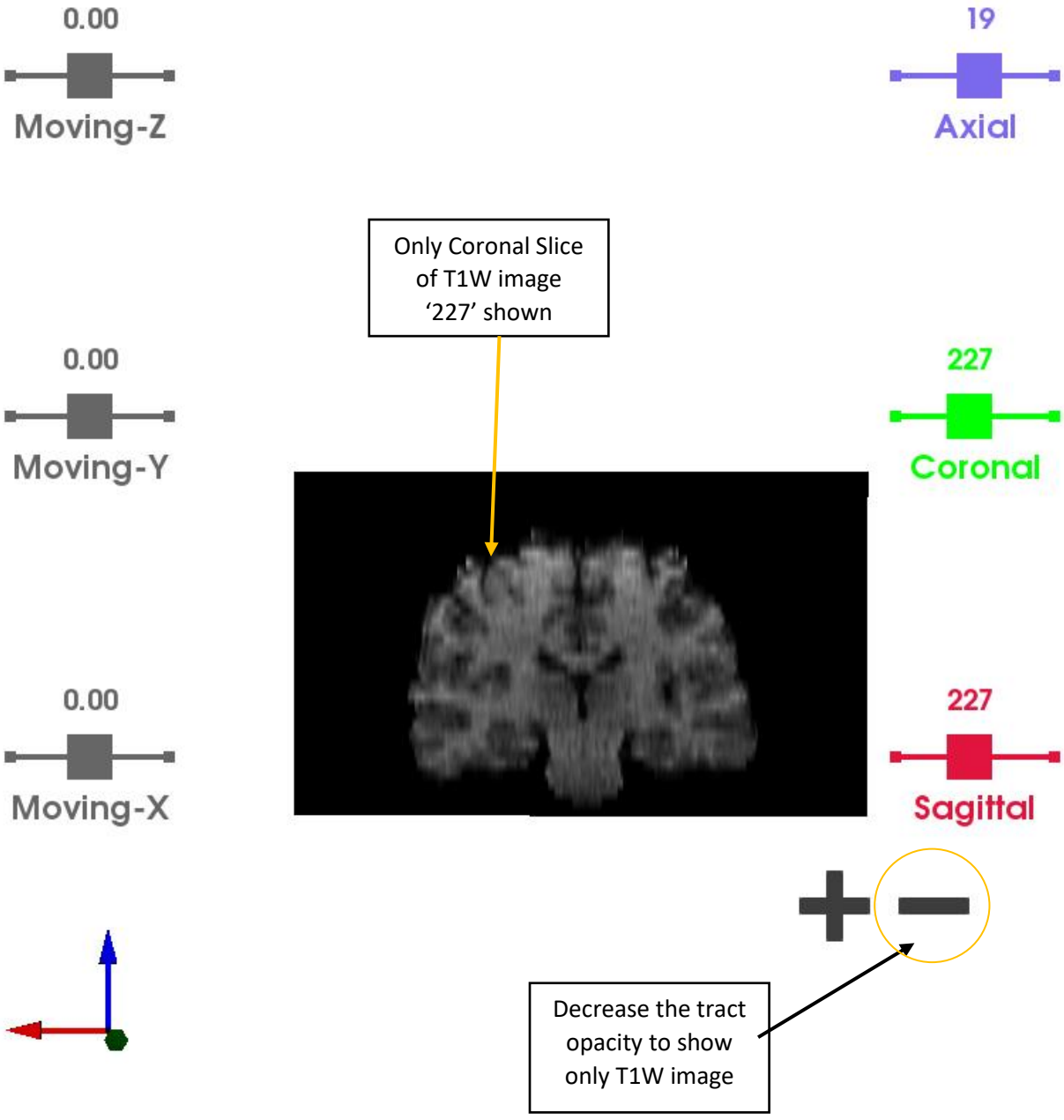

Figure 46: Integral Visualization Tool (Part 5)

4.4 Fiber Bundles Clustering Interpretation

Clustering allows the bundle of interest (BOI) to be analyzed further in small scale quantity of fibers. This interface demonstrates the result of fiber clustering. It contains the clustered BOI along with its centroids. By default, it shows only the centroids. When the next or previous button is pressed, the pertinent cluster is shown. With this interface, any loss of one or two or more axonal tracts that belongs to the BOI can be detected with ease, by comparing it to the streamlines of healthy subjects.

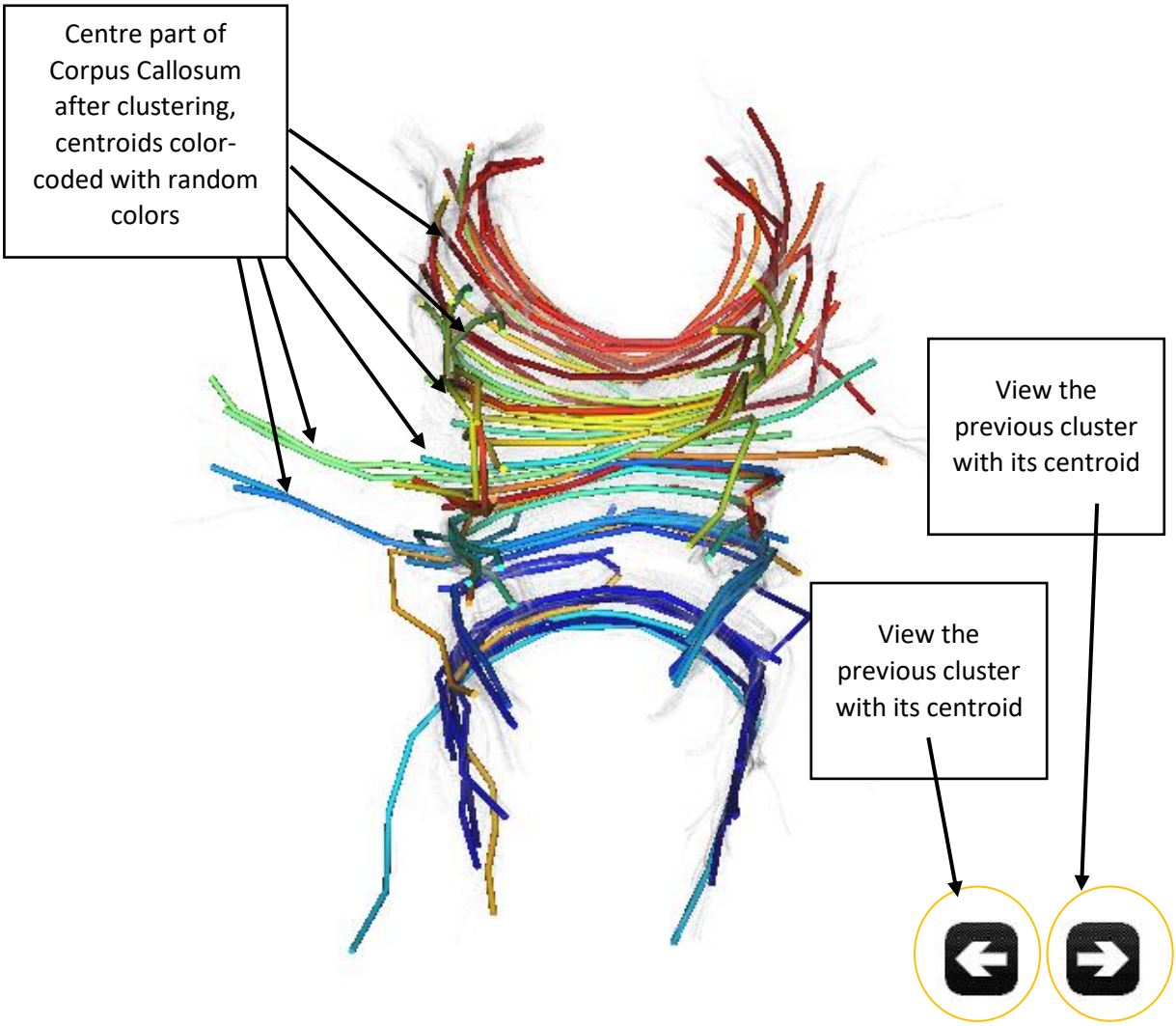

Figure 47: Clustering Observational Study (Part 1)

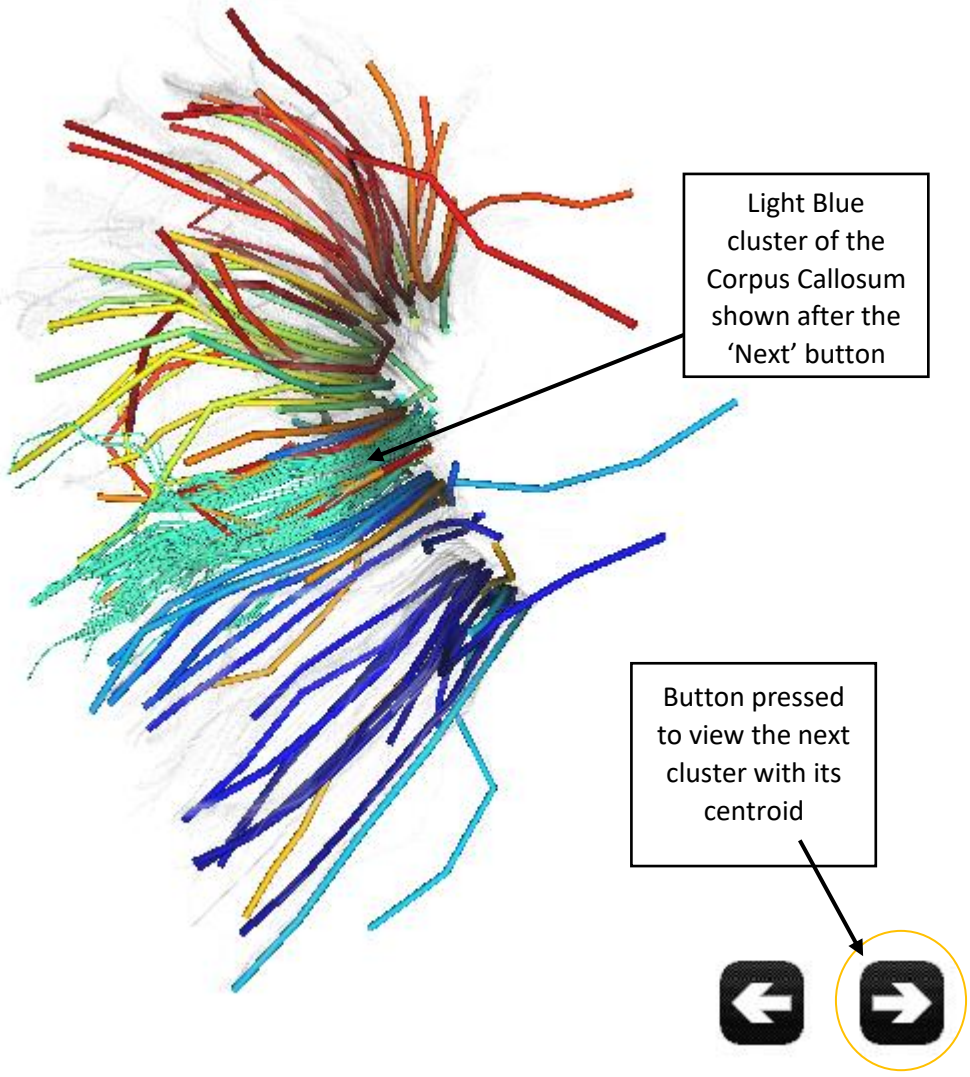

Figure 48: Clustering Observational Study (Part 2)

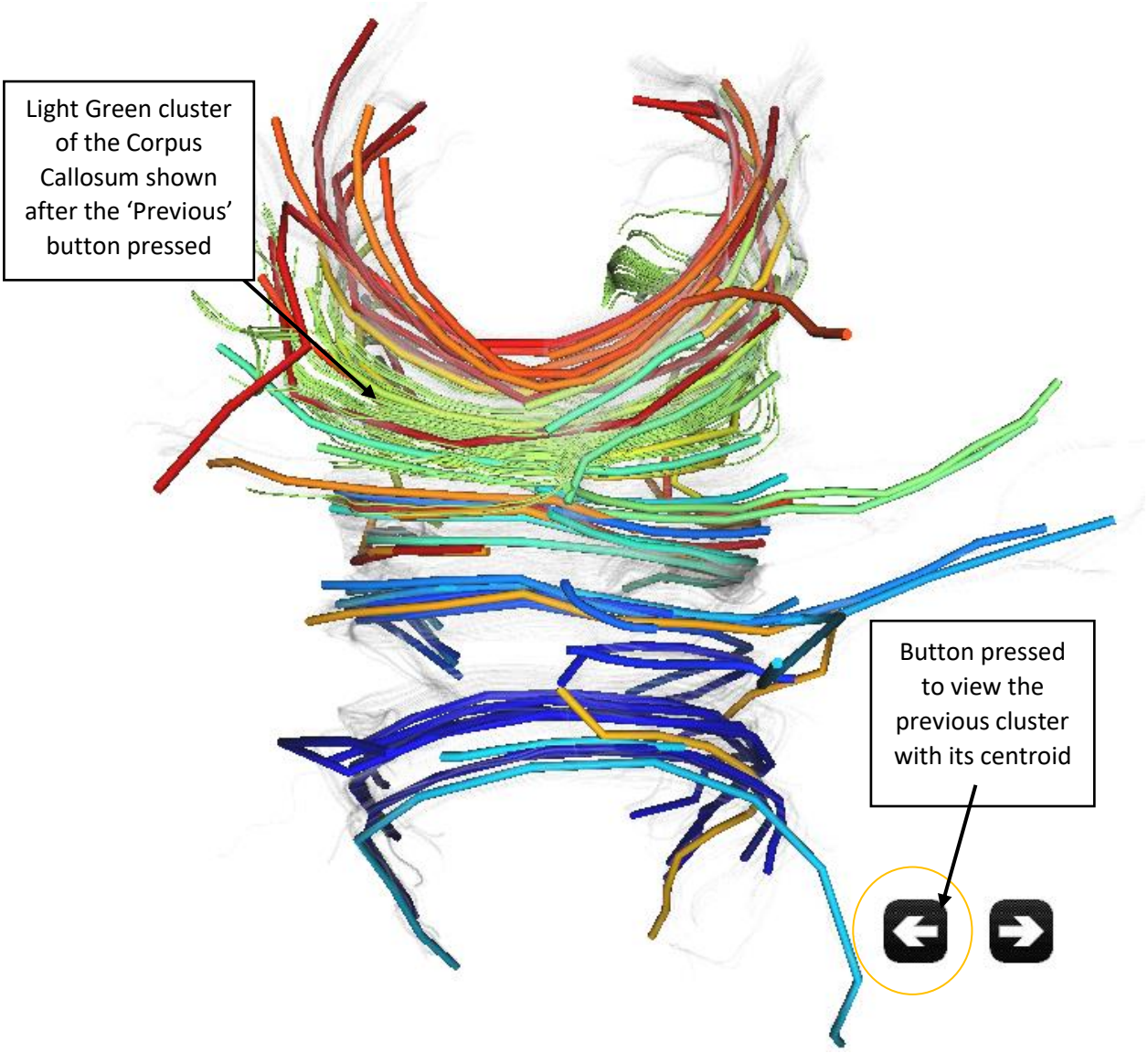

Figure 49: Clustering Observational Study (Part 3)

4.5 Differential Study on Fiber Bundles

Conventional differential study across the T1W images is not strong enough to find the neuroimaging biomarker. The differential study across the different subjects' fiber bundles of interest (BOI) can be one step further to enhance the discover of potential WM neuroimaging biomarkers by comparing the relative tract length and tract density. For this purpose, an interface is developed to compare the BOIs of the healthy and the 'Ketum' groups. This interface can support up to 5 BOIs for differential study. The BOIs is color-coded in the red, green, blue, yellow and neon blue. Colored with the same color as the BOIs, its corresponding slider widget is to move the BOIs leftwards and rightwards to superimpose together with others for quantitative comparison.

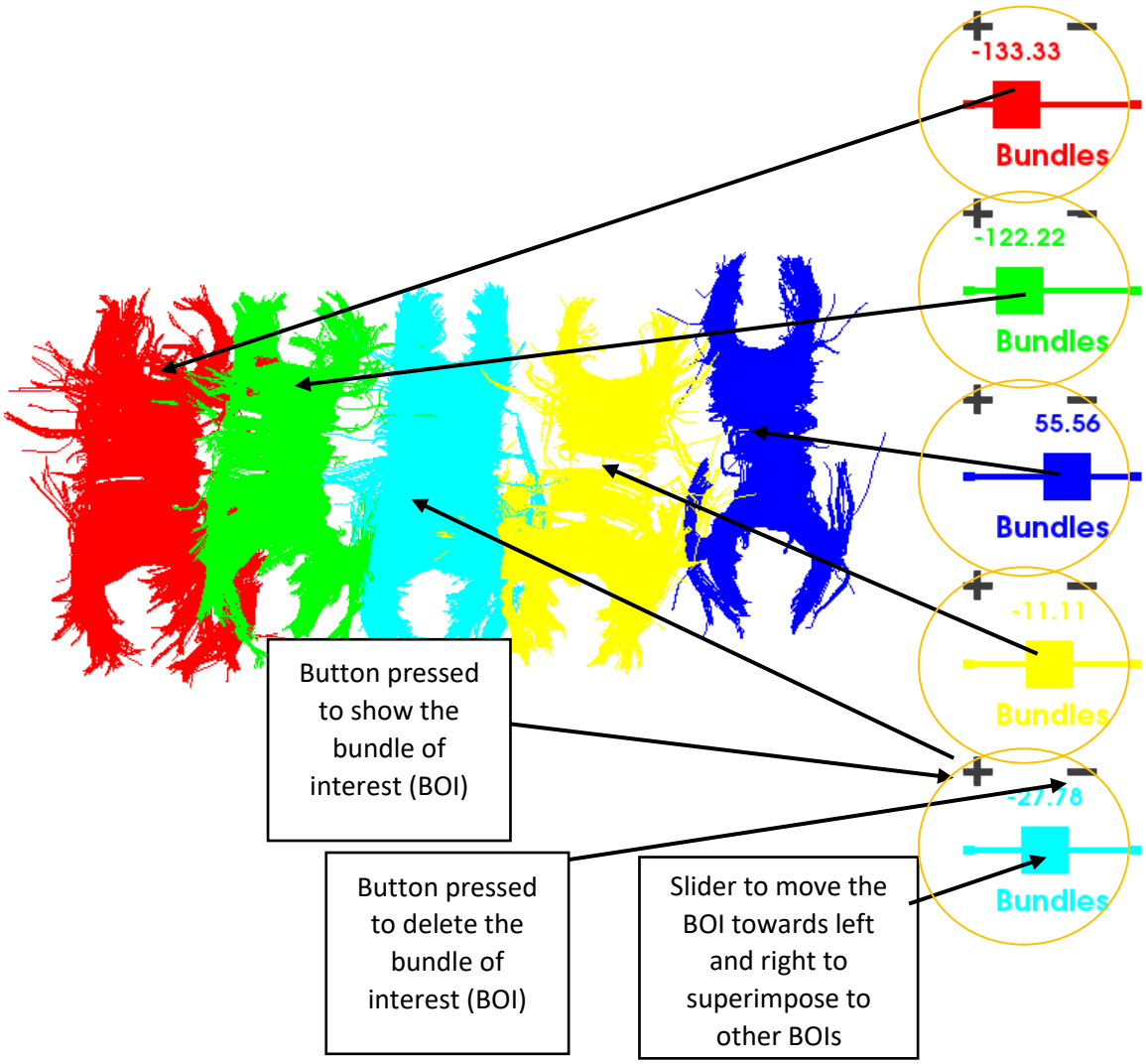

Figure 50: WM Differential Study (Part I)

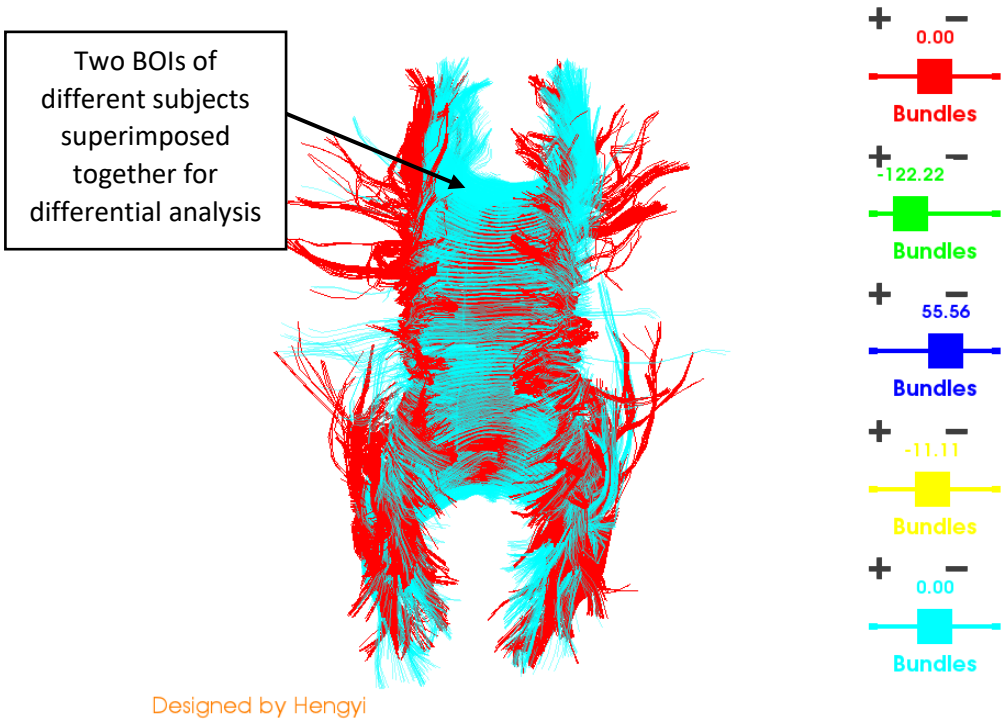

Figure 51: WM Differential Study (Part II)

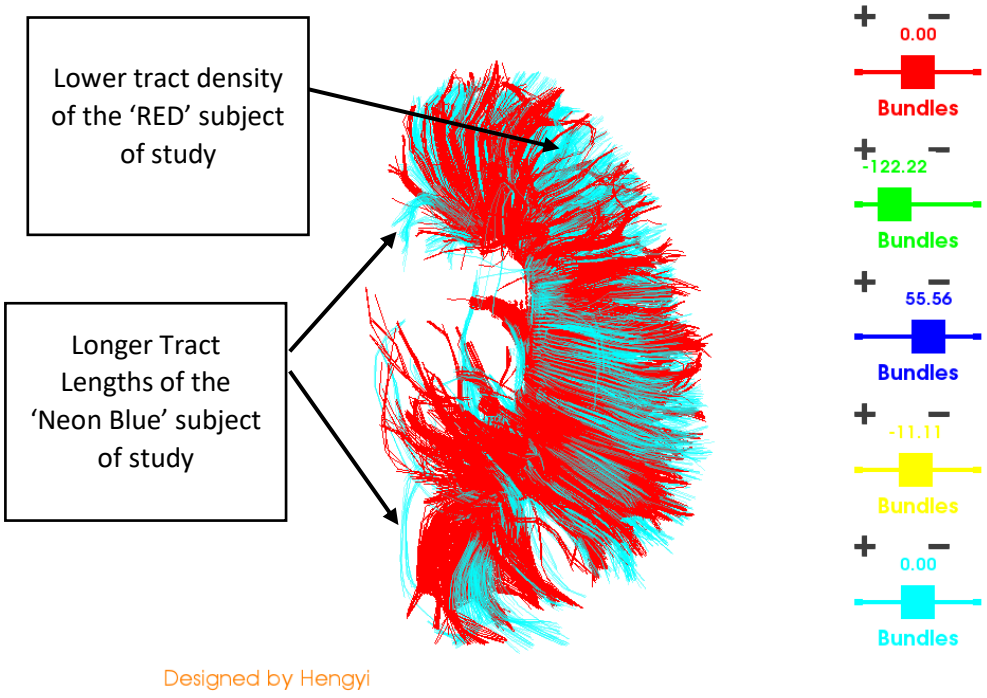

Figure 52: WM Differential Study (Part III)

4.4 Fiber Length and Connectivity Metrics Analysis

With all the WM tracts, it is interested to group them in regions-of-interest(ROI) for surfaces and volumes. The regions are based on the aparc+aseg.mgz label map generated by FreeSurfer and are modified to create 89 regions of interest. Each region is associated with the subcortical structure of the cerebral cortex. To begin, the white matter voxel from the streamlines is filtered out with the label of 1 or 2. To have only the corpus callosum as the region of interest, the label value of 2 is used as the ROI parameter. After grouping the WM tracts in the ROIs, the connectivity matrix is plotted to show the connectivity among the subcortical regions. In other words, the total number of streamlines are counted based on the tracts that connect from the region A to region B.

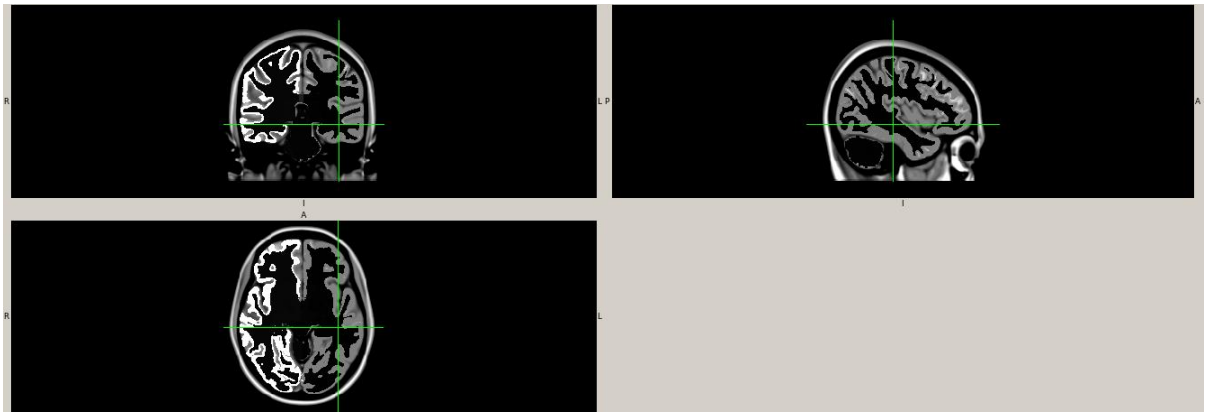

Figure 53: White matter labelled as 2 is segmented (shown in dark shaded region), overlapping with the MNI152 subject.

Healthy and 'Ketum' Group Connectivity Metrics

The connectivity metrics are plotted across the healthy and the 'Ketum' drug addiction subjects. The color legend in the metrics indicates the magnitude of the quantity of the streamlines connecting among the subcortical regions that have been assigned early the labels from integers '2' to '88'. Increasing color intensity starting from blue towards red indicates increasing magnitude.

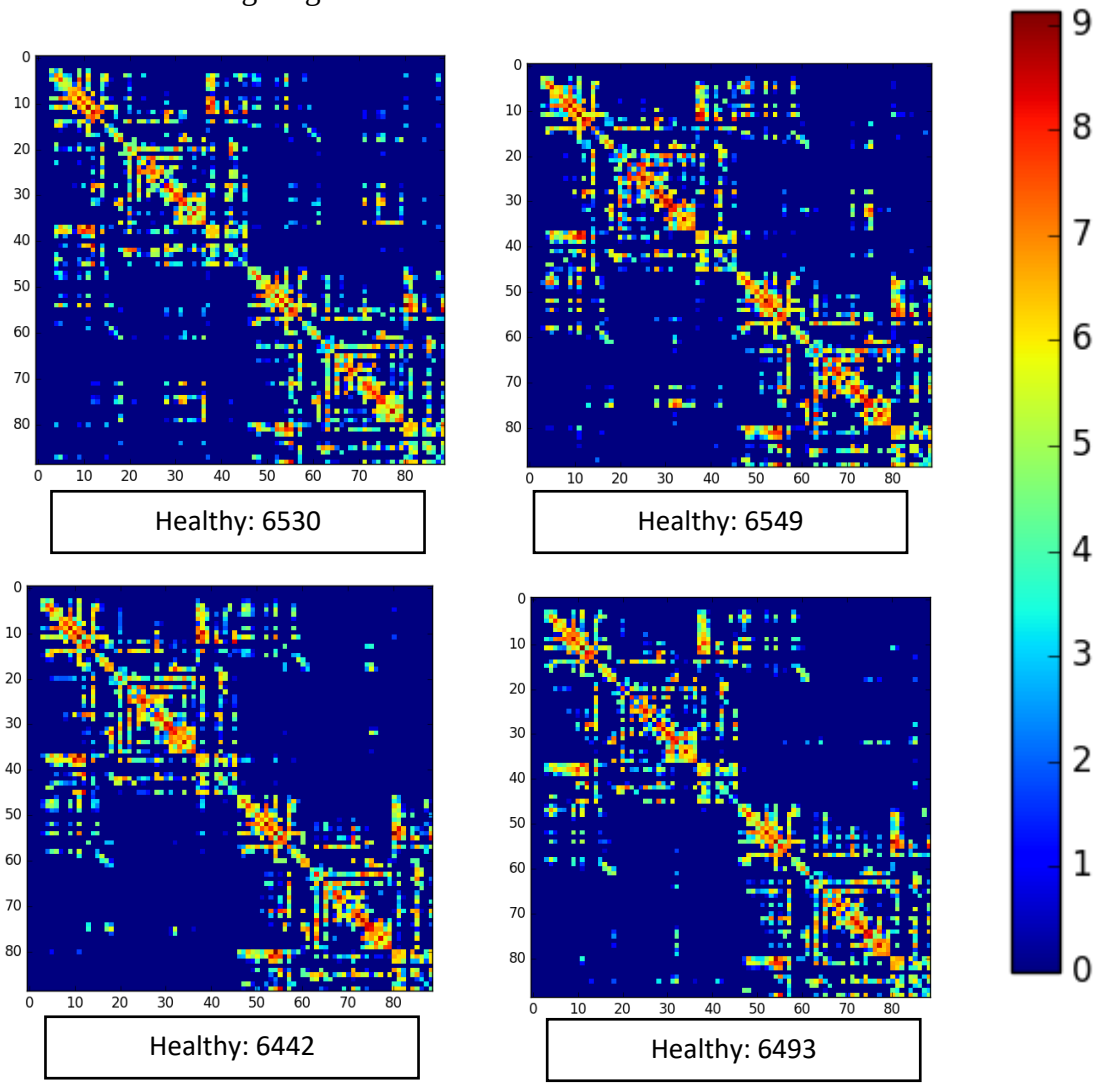

Figure 54: Connectivity Metrics (Part 1)

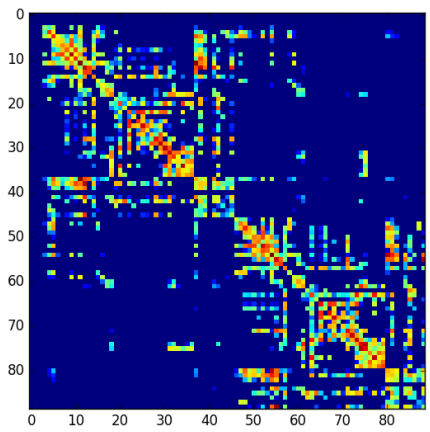

Healthy: 6571

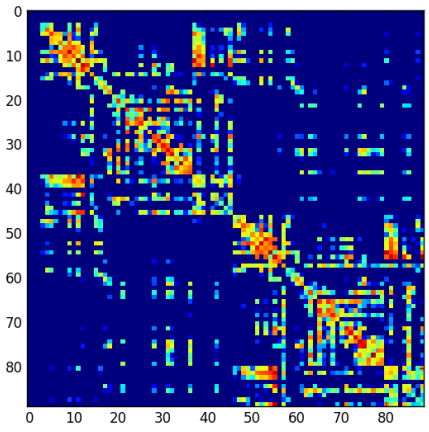

Ketum: 6443

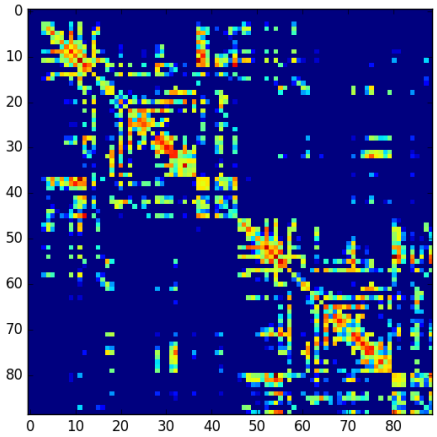

Ketum: 6308

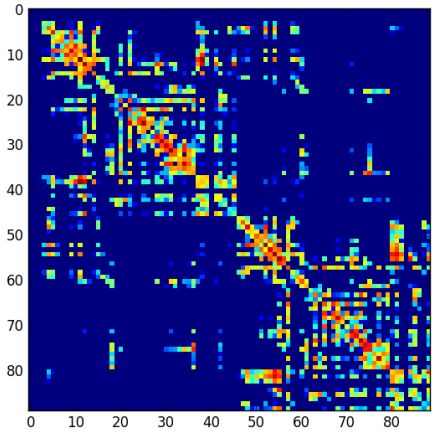

Ketum: 6350

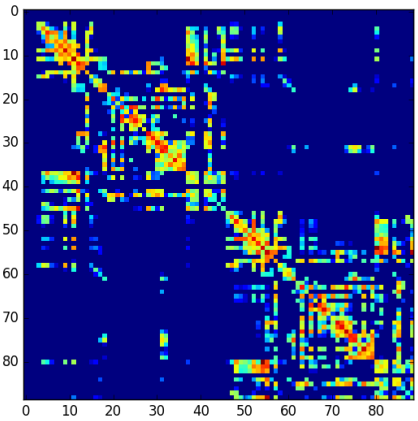

Ketum: 6297

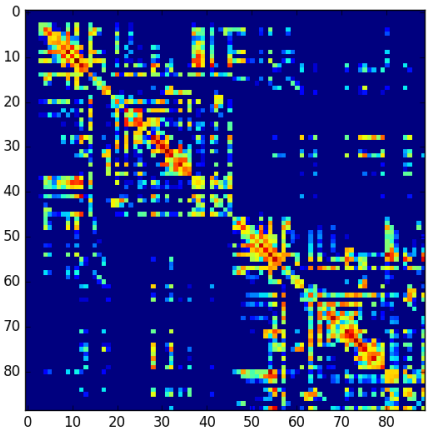

Ketum: 6375

Figure 55: Connectivity Metrics (Part 2)

Length Count of Corpus Callosum in Healthy and 'Ketum' Groups

Analyzing the length in millimeter on the bundle of interest (BOI) is a crucial step to discover any damage to the WM microstructures, besides performing quantitative analysis on the BOI in the early step of the differential study. The length(mm) of the corpus callosum as the BOI across all the subjects are plotted in histograms. It is noticeable that the short length (0-10mm) of the streamlines are the most in the corpus callosum, regardless the subjects of study.

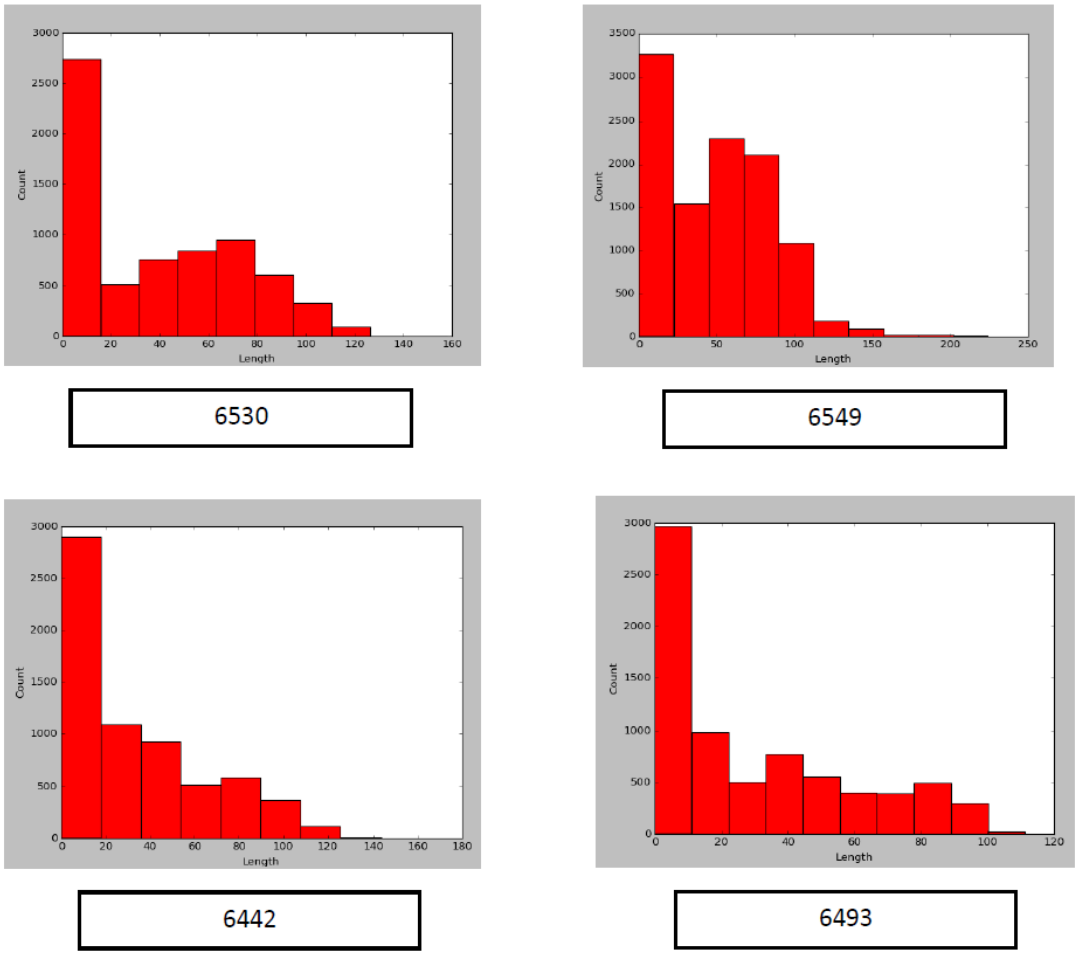

Figure 56: Length Count (Part 1)

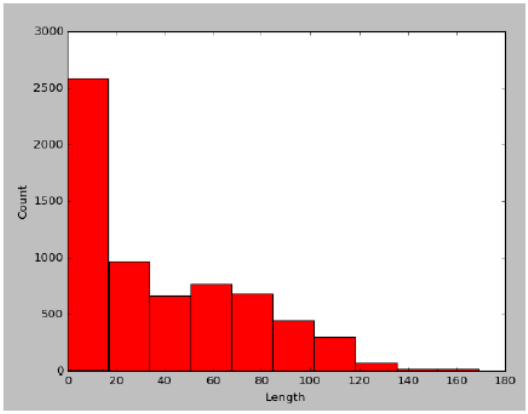

6571

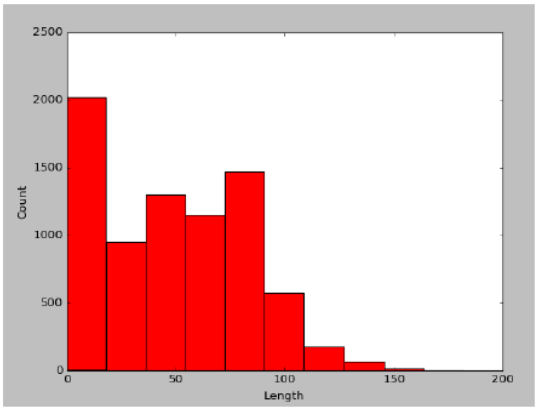

6443

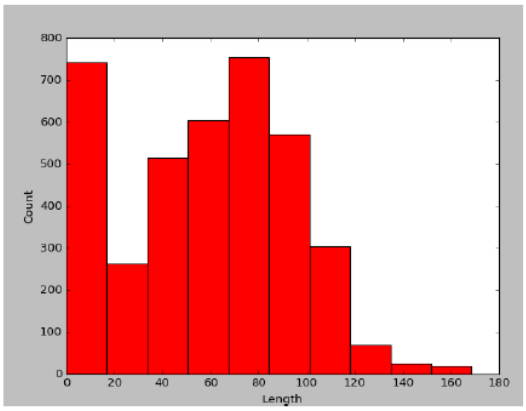

6308

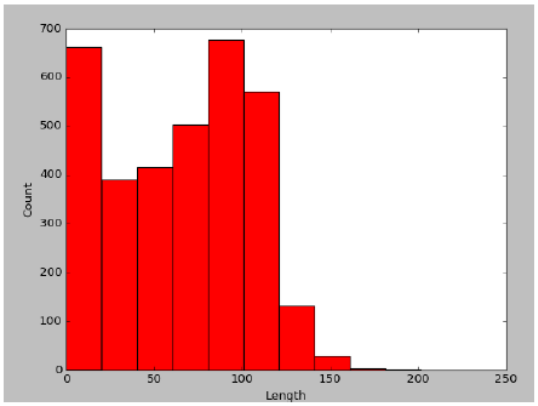

6350

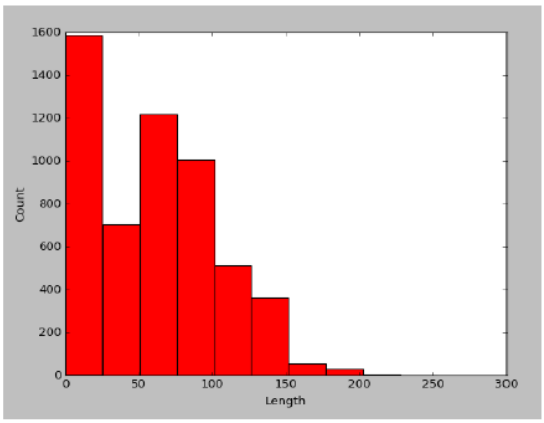

6297

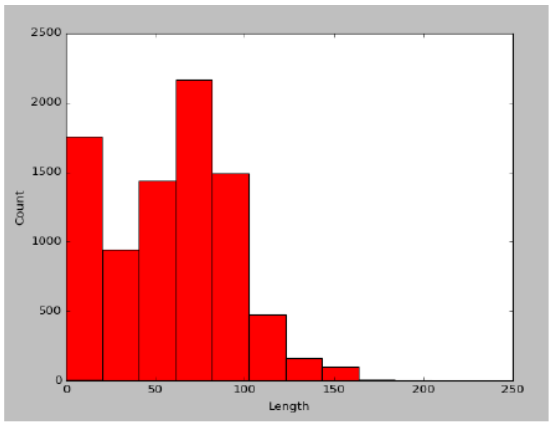

6375

Figure 57: Length Count (Part 2)

4.6 Tract-Based Spatial Statistics (TBSS)

TBSS is used to analyze the DTI data between two groups of subjects. They are the control group of 5 healthy subjects with a group of 5 ‘Ketum’ drug addiction subjects. The fractional anisotropy (FA) images of each subject are constructed using the Dipy library and are used as the inputs in TBSS analysis. The TBSS is performed via FSL tool. The objective is to figure out the areas where the WM tract skeleton between two groups of subjects are remarkably different. The very first step in TBSS is to eliminate the brain-edge artefacts and zero the end slices, by running the tbss_1_preproc algorithm. Next, all the FA data across the subjects are registered in the 1mm x 1mm x1mm standard space called the Montreal Neurological Institute (MNI) space. In post-registration step, all the subject’s standard space nonlinearly aligned images are integrated into one 4D image file. The subsequent step in TBSS is to project all pre-aligned FA data onto the skeleton, by thresholding the mean FA skeleton image at 0.3 to create the binary skeleton mask for next step processing. Last, it is to run the voxelwise statistics on the skeletonized FA data. The generated result is overlapped with the standard space called MNI152_T1_1mm provided by the FSL tool. As shown in the Figure 58, it is remarkable that the presence of small ‘RED’ regions suggests that there is global decrease in FA with ‘Ketum’ drug addiction.

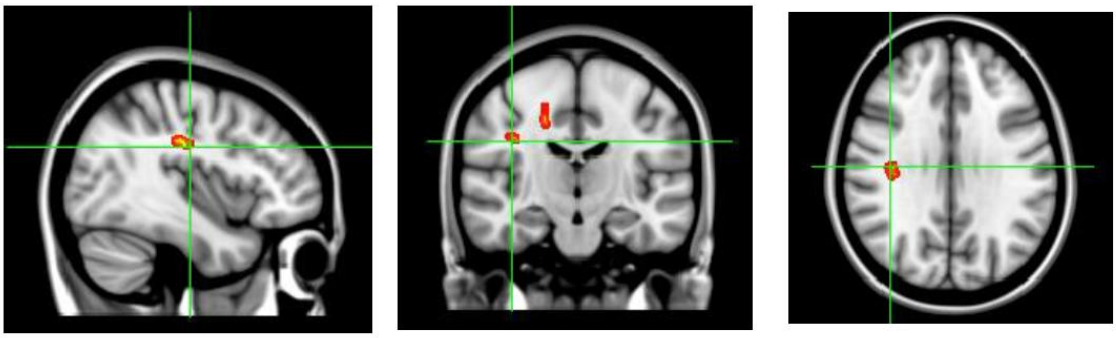

Figure 58: (Left: Sagittal, Middle: Coronal, Right: Axial) Slices Containing the Affected Regions

To find out where the small ‘Red’ regions that encounter the global decrease of FA as a result of the effect of ‘Ketum’ drug addiction, a metric is created to map the ‘Red’ regions. The metric measures the regions based on the subcortical regions defined early by the freesurfer labels. In other words, each label or each integer number indicates a subcortical region in the human brain. To represent 3025 labels in metric, it is the sum of the x and y integers that tells the specific label. The color intensity in the metric begins from white and increases towards dark blue. It suggests the severity of the particular affected region. Dark blue indicates that the subcortical region encounters the highest global decrease of FA, whereas the white color indicates that the region is not affected. By mapping the small ‘Red’ region into the developed metric, it is found out that the subcortical region of precentral cortex on left hemisphere is affected the most, by relating the label of 1024 to the defined freesurfer label provided in appendix, after summing up the numbers of 990 and 34. This is followed by the subcortical regions of cortex in left hemisphere of caudalmiddlefrontal (1003), postcentral (1022), and superiorfrontal (1028), shown in Figure 59.

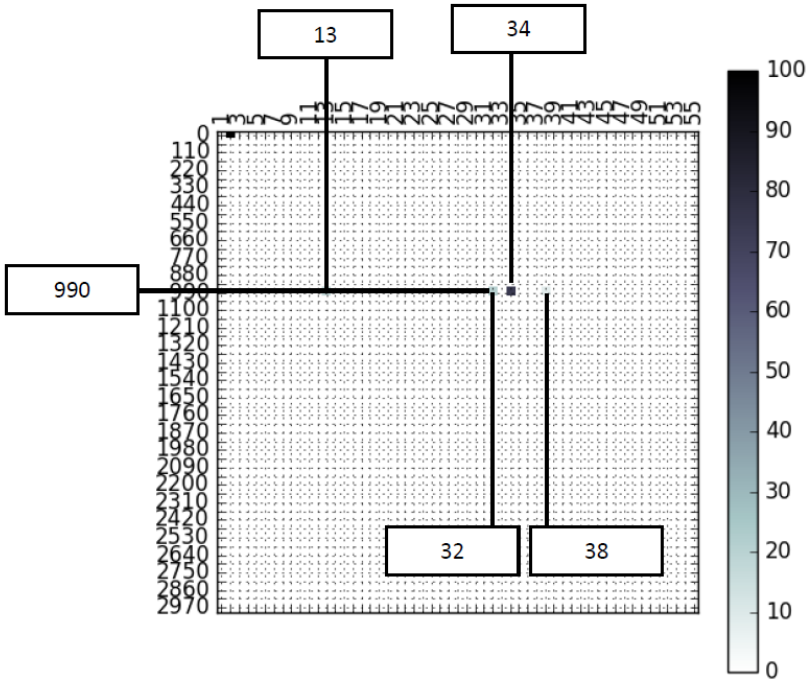

Figure 59: Affected Regions Metric (FA)

Besides FA map, the Geodesic Anisotropy (GA) map is also famous to be used as the scalar measures of fiber integrity. Hence, similar procedures of TBSS is performed, but the inputs are the GA images of 5 healthy subjects and a group of 5 ‘Ketum’ drug addiction subjects. The objective is same to find out the global decrease of GA between two groups. With the generated result of the voxelwise statistical analysis performed via TBSS, it is mapped into the metric which shows the affected subcortical regions based on the intensity values. As shown in the Figure 60, the metric shows that the subcortical region of precentral cortex on left hemisphere is again affected the most, indicated as ‘1024’ in the freesurfer label. This result is identical to the result presented early using the FA images as the input to TBSS. Not only the ‘1024’ subcortical region is found out to be affected by the effect of ‘Ketum’ drug addiction in both FA and GA, but also the subcortical regions of cortex in left hemisphere of caudal-middle-frontal (1003) and superior-frontal (1028).

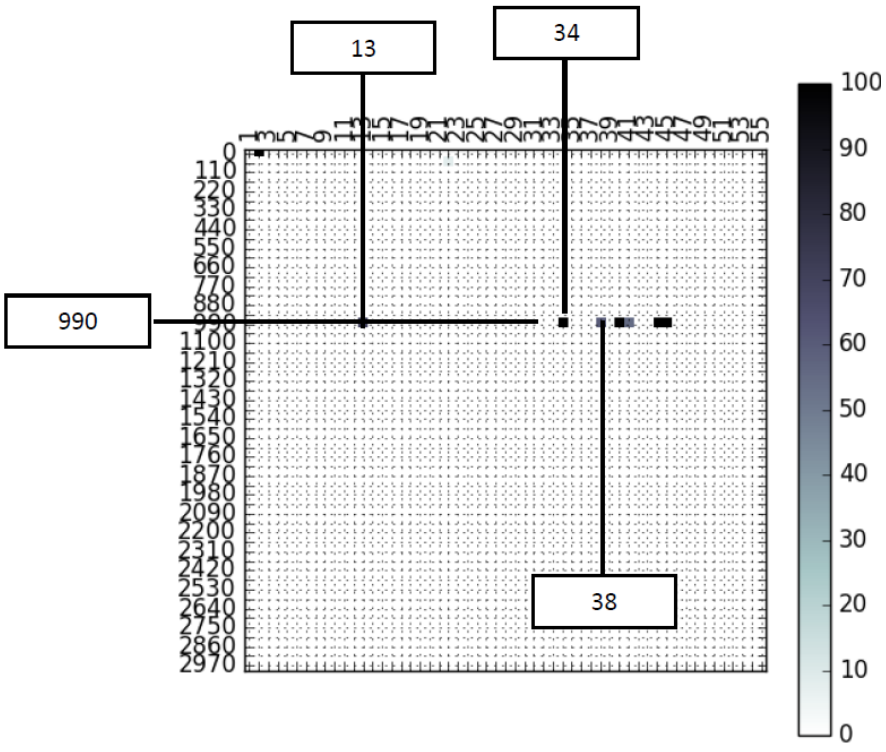

Figure 60: Affected Region Metric (GA)

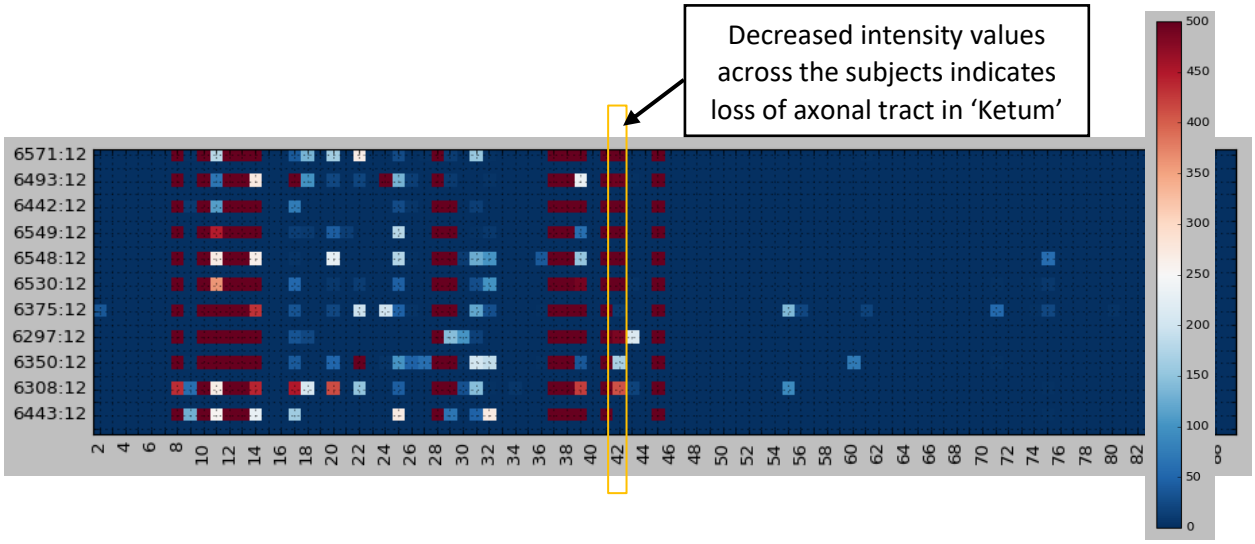

Figure 61: TBSS Connectivity Metric

The left hemisphere of cortex precentral in 'Ketum' subject group is found out to encounter global decrease in the FA and the GA, compared to the healthy group. In other words, there is significant loss of axonal tracts that pass across this subcortical region. To further find out the tracts where they connect to, begin from the left hemisphere of cortex precentral, another metric is plotted out. This metric takes all the WM structures that belongs to different subjects of the healthy group and the 'Ketum' drug addiction group, generated early in WM tractography steps. The healthy subjects are the 6571, 6493, 6442, 6549, 6548, 6530, whereas the 'Ketum' drug addiction subjects are 6375, 6297, 6350, 6308, and 6443. Next, the metric indicates the left hemisphere of cortex precentral as the new label of '12' with the respective subjects in its left, whereas the bottom of the metric indicates the 89 latest defined labels of subcortical regions. These new redefined labels can be found in the Appendix. As shown in the Figure 61, the intensity values in the column 42 decreases from red towards blue. This suggests that the healthy group possesses higher number of axonal tracts compared to the 'Ketum' drug addiction group. These tracts are connecting from the left hemisphere of cortex precentral to the subcortical region of left hippocampus, indicated as the new label '42'. The decline in the density of axonal tracts connecting from the left-hemisphere of cortex precentral that locates in the frontal lobe to the left hippocampus is the biomarker of the dementia caused by the 'Ketum' drug addiction. This result is evidently proven by the analysis of electroencephalogram (EEG) that has been performed by the USM [35],

which has also shown profound cognitive impairments in the hippocampus and the electrocorticography (ECoG) of the frontal cortex [35].

5.0 CONCLUSION

Memory loss is considered a symptom of dementia. The major root causes of the dementia are neurodegenerative diseases. Nonetheless, drug addiction also renders the dementia. Based on the preclinical study on the effect of 'Ketum' drug addiction [35], the chronic mitragynine administration extracted from the 'Ketum' plant led to impaired learning and memory. This is evident by the analysis of electroencephalogram (EEG) that has shown profound cognitive impairments in the hippocampus and the electrocorticography (ECoG) of the frontal cortex [35]. To locate the potential biomarker caused by the 'Ketum' drug addiction, these findings have developed several neuroimaging examinations in the easy-used graphical user interface (GUI). It includes an integral visualization of 3D WM geometry and structure with the 2D T1W images, a differential diagnosis of the WM of two-sample subjects as the complement to enhance the evidence of biomarker potential, and the TBSS of diffusion tensor Fractional Anisotropy (FA) and Geodesic Anisotropy (GA). Lack of a neuroimaging specialist in this research study is the hindrance to achieve a great result with the first two developed algorithms. Besides, the datasets that are not in the High Angular Resolution Diffusion Imaging (HARDI) format are the factors that decrease the resolution of WM reconstruction. Nonetheless, the TBSS with the two widely-used scalar measures of FA and GA has proven that the axonal tracts in the subcortical regions of left hemisphere of cortex precentral, caudal-middle-frontal, and superior-frontal decrease. Moreover, it is discovered that the axonal tracts connecting from the left-hemisphere of cortex precentral to the subcortical region of the left hippocampus in the 'Ketum' drug addiction group are lesser, compared the healthy group. It is concluded that the decline in the tract density in these subcortical regions are the potential WM neuroimaging biomarkers that have caused the profound impairments in learning and memory in 'Ketum' drug addicted subjects.

6.0 REFERENCES

[1] Alexander, A. L., Lee, J. E., Lazar, M., & Field, A. S. (2007). Diffusion tensor imaging of the brain. *Neurotherapeutics, 4*(3), 316-329.

[2] Assaf, Y., & Pasternak, O. (2008). Diffusion tensor imaging (DTI)-based white matter mapping in brain research: a review. *Journal of Molecular Neuroscience, 34*(1), 51-61.

[3] Basser, P. J., & Jones, D. K. (2002). Diffusion-tensor MRI: theory, experimental design and data analysis–a technical review. *NMR in Biomedicine, 15*(7-8), 456-467.

[4] Basser, P. J., Mattiello, J., & LeBihan, D. (1994). MR diffusion tensor spectroscopy and imaging. *Biophysical journal, 66*(1), 259.

[5] Bernstein, M. A., King, K. F., & Zhou, X. J. (2004). *Handbook of MRI pulse sequences*: Elsevier.

[6] Bickle et al. (n.d.). *Diffusion Tensor Imaging*. Retrieved October 16, 2016, from *https://radiopaedia.org/articles/diffusion-tensor-imaging*

[7] Buism. (2013). *The Fundamental Difference between Men and Women, Part 1: Neurons.* Retrieved October 16, 2016, from *http://buism.com/neurons.htm*

[8] Freudenrich,C.,&Boyd,R.(2001, June 6). *How Your Brain Works*. Retrieved October 16, 2016, from *http://science.howstuffworks.com/life/inside-the-mind/human-brain/brain1.htm*

[9] Gailard et al. (n.d.). *MRI Pulse Sequence*. Retrieved October 16, 2016, from *https://radiopaedia.org/articles/mri-pulse-sequences-1*

[10] Geobel, R. (2014). *Diffusion-Weighted Imaging Analysis*. Retrieved October 16, 2016, from *http://www.brainvoyager.com/bvqx/doc/UsersGuide/DWI/DiffusionWeightedImagingAnalysis.html*

[11] Golman, K., Axelsson, O., & Johannesson, H. (2003). Magnetic resonance imaging: Google Patents.

[12] Kingsley, P. B. (2006). Introduction to diffusion tensor imaging mathematics: Part I. Tensors, rotations, and eigenvectors. *Concepts in Magnetic Resonance Part A, 28*(2), 101-122.

[13] Kingsley, P. B. (2006). Introduction to diffusion tensor imaging mathematics: Part II. Anisotropy, diffusion-weighting factors, and gradient encoding schemes. *Concepts in Magnetic Resonance Part A, 28*(2), 123-154.

[14] Kingsley, P. B. (2006). Introduction to diffusion tensor imaging mathematics: Part III. Tensor calculation, noise, simulations, and optimization. *Concepts in Magnetic Resonance Part A, 28*(2), 155-179.

[15] Kniple et al. (n.d.). *Diffusion Weighted Imaging*. Retrieved October 16, 2016, from *https://radiopaedia.org/articles/diffusion-weighted-imaging-1*

[16] Legazpi, G.A., & Lingo, A.J. (2016, October 03). *What is the Difference Between White Matter and Grey Matter?*. Retrieved October 16, 2016, from *http://www.wisegeek.com/what-is-the-difference-between-white-matter-and-grey-matter.htm*

[17] Makris, N., Papadimitriou, G., Worth, A., Jenkins, B. G., Garrido, L., Sorensen, A. G., . . . Cudkowicz, M. E. (2002). Diffusion tensor imaging. *Neuropsychopharmacology: the fifth generation of progress. New York: Lippincott, Williams, and Wilkins*, 357-371.

[18] Mori, S., & Zhang, J. (2006). Principles of diffusion tensor imaging and its applications to basic neuroscience research. Retrieved October 16, 2016, from *http://www.sciencedirect.com/science/article/pii/S0896627306006349*

[19] Mukherieea, P. (2008, March 13). *Diffusion Tensor MR Imaging and Fiber Tractography: Theory Underpinnings*. Retrieved October 16, 2016, from *http://www.ajnr.org/content/29/4/632.full*

[20] NAIMA. (2014, November 8). *Different Between Grey Matter and White Matter*. Retrieved October 16, 2016, from *http://www.differencein.com/difference-between-grey-matter-and-white-matter/*

[21] National Institute of Neurological Disorders and Stroke. (2015, April 17). *Brain Basic: Know Your Brain.* Retrieved October 16, 2016, from *http://www.ninds.nih.gov/disorders/brain_basics/know_your_brain.htm*

[22] Pajevic, S., & Pierpaoli, C. (1999). Color schemes to represent the orientation of anisotropic tissues from diffusion tensor data: application to white matter fiber tract mapping in the human brain. *Magnetic resonance in medicine, 42*(3), 526-540.

[23] Serendip. (2012, September 05). *Brain Structures and their Functions*. Retrieved October 16, 2016, from *http://serendip.brynmawr.edu/bb/kinser/Structure1.html*

[24] Stejskal, E. O., & Tanner, J. E. (1965). Spin diffusion measurements: spin echoes in the presence of a time-dependent field gradient. *The journal of chemical physics, 42*(1), 288-292.

[25] Abhinav, K., Yeh, F.-C., Pathak, S., Suski, V., Lacomis, D., Friedlander, R. M., & Fernandez-Miranda, J. C. (2014). Advanced diffusion MRI fiber tracking in neurosurgical and neurodegenerative disorders and neuroanatomical studies: A review. *Biochimica et Biophysica Acta (BBA)-Molecular Basis of Disease, 1842*(11), 2286-2297.

[26] Catani, M., & de Schotten, M. T. (2008). A diffusion tensor imaging tractography atlas for virtual in vivo dissections. *Cortex, 44*(8), 1105-1132.

[27] Chekir, A., Descoteaux, M., Garyfallidis, E., Côté, M.-A., & Boumghar, F. O. (2014). *A hybrid approach for optimal automatic segmentation of White Matter tracts in HARDI*. Paper presented at the Biomedical Engineering and Sciences (IECBES), 2014 IEEE Conference on.

[28] DSI Studio. (n.d.). *Diffusion MRI Fiber Tracking*. Retrieved December 4, 2016, from *http://dsi-studio.labsolver.org/course/fiber-orientation-distribution*

[29] Lawes, I. N. C., Barrick, T. R., Murugam, V., Spierings, N., Evans, D. R., Song, M., & Clark, C. A. (2008). Atlas-based segmentation of white matter tracts of the human brain using diffusion tensor tractography and comparison with classical dissection. *Neuroimage, 39*(1), 62-79.

[30] Mukherjee, P., Berman, J., Chung, S., Hess, C., & Henry, R. (2008). Diffusion tensor MR imaging and fiber tractography: theoretic underpinnings. *American journal of neuroradiology, 29*(4), 632-641.

[31] Yeh, F.-C., Verstynen, T. D., Wang, Y., Fernández-Miranda, J. C., & Tseng, W.-Y. I. (2013). Deterministic diffusion fiber tracking improved by quantitative anisotropy. *PloS one, 8*(11), e80713.

[32] Zhang, Y., Zhang, J., Oishi, K., Faria, A. V., Jiang, H., Li, X., . . . Evans, A. (2010). Atlas-guided tract reconstruction for automated and comprehensive examination of the white matter anatomy. *Neuroimage, 52*(4), 1289-1301.

[33] Frisoni, G. B., Fox, N. C., Jack, C. R., Scheltens, P., & Thompson, P. M. (2010). The clinical use of structural MRI in Alzheimer disease. Nature Reviews Neurology, 6(2), 67-77.

[34] Das, S. R., Mechanic-Hamilton, D., Korczykowski, M., Pluta, J., Glynn, S., Avants, B. B., . . . Yushkevich, P. A. (2009). Structure specific analysis of the hippocampus in temporal lobe epilepsy. Hippocampus, 19(6), 517.

[35] Yusoff, N. H., Suhaimi, F. W., Vadivelu, R. K., Hassan, Z., Rümler, A., Rotter, A., . . . Navaratnam, V. (2016). Abuse potential and adverse cognitive effects of mitragynine (kratom). Addiction biology, 21(1), 98-110.

[36] Tripathi, M., & Vibha, D. (2009). Reversible dementias. Indian Journal of Psychiatry, 51(Suppl1), S52–S55.

[37] Zivadinov, R., Stosic, M., Cox, J. L., Ramasamy, D. P., & Dwyer, M. G. (2008). The place of conventional MRI and newly emerging MRI techniques in monitoring different aspects of treatment outcome. Journal of neurology, 255, 61-74.

[38] Caeyenberghs, K., & Leemans, A. (2014). Hemispheric lateralization of topological organization in structural brain networks. Human brain mapping, 35(9), 4944-4957.

[39] Subcortical Segmentation. (n.d.). Retrieved March 17,2017 from http://freesurfer.net/fswiki/SubcorticalSegmentation

[40] Fischl, B., Salat, D. H., Busa, E., Albert, M., Dieterich, M., Haselgrove, C., . . . Klaveness, S. (2002). Whole brain segmentation: automated labeling of neuroanatomical structures in the human brain. *Neuron, 33*(3), 341-355.

[41] Magnetic Resonance Imaging (MRI) of the Brain and Spine: Basics. (n.d.). Retrieved March20,2017 from

http://casemed.case.edu/clerkships/neurology/Web%20Neurorad/MRI%20Basics.htm

[42] Hanke, M., Baumgartner, F. J., Ibe, P., Kaule, F. R., Pollmann, S., Speck, O., . . . Stadler, J. (2014). A high-resolution 7-Tesla fMRI dataset from complex natural stimulation with an audio movie. Scientific data, 1.

[43] Education.Whats an MRI. (2015). Retrieved April 2,2017 from http://multiple-sclerosis-research.blogspot.com/2015/01/education-whats-mri.html

[44] Soares, J., Marques, P., Alves, V., & Sousa, N. (2013). A hitchhiker's guide to diffusion tensor imaging. Frontiers in neuroscience, 7, 31.

[45] Madden, D. J., Bennett, I. J., Burzynska, A., Potter, G. G., Chen, N.-k., & Song, A. W. (2012). Diffusion tensor imaging of cerebral white matter integrity in cognitive aging. Biochimica et Biophysica Acta (BBA)-Molecular Basis of Disease, 1822(3), 386-400.

[46] Alexander, A. L., Lee, J. E., Lazar, M., & Field, A. S. (2007). Diffusion tensor imaging of the brain. Neurotherapeutics, 4(3), 316-329.

[47] The diffusion tensor, and its relation to FA, MD, AD and RD. (2015). Retrieved on April 5,2017 from http://www.diffusion-imaging.com/2015/10/what-is-diffusion-tensor.html

[48] Batchelor, P., Moakher, M., Atkinson, D., Calamante, F., & Connelly, A. (2005). A rigorous framework for diffusion tensor calculus. Magnetic resonance in medicine, 53(1), 221-225.

[49] Garyfallidis, E., Brett, M., Amirbekian, B., Rokem, A., Van Der Walt, S., Descoteaux, M., & Nimmo-Smith, I. (2014). Dipy, a library for the analysis of diffusion MRI data. Frontiers in neuroinformatics, 8, 8.

[50] Cluster analysis. (2017). In Wikipedia, The Free Encyclopedia. Retrieved 08:23, April 17, 2017, from https://en.wikipedia.org/wiki/Cluster_analysis

[51] Schwarz, C. G., Reid, R. I., Gunter, J. L., Senjem, M. L., Przybelski, S. A., Zuk, S. M., . . . Kantarci, K. (2014). Improved DTI registration allows voxel-based analysis that outperforms tract-based spatial statistics. Neuroimage, 94, 65-78.

[52] S.M. Smith, M. Jenkinson, H. Johansen-Berg, D. Rueckert, T.E. Nichols, C.E. Mackay, K.E. Watkins, O. Ciccarelli, M.Z. Cader, P.M. Matthews, and T.E.J.

Behrens. Tract-based spatial statistics: Voxelwise analysis of multi-subject diffusion data. NeuroImage, 31:1487-1505, 2006.

[53] J.L.R. Andersson, M. Jenkinson and S. Smith. Non-linear optimisation. FMRIB technical report TR07JA1 from www.fmrib.ox.ac.uk/analysis/techrep

[54] J.L.R. Andersson, M. Jenkinson and S. Smith. Non-linear registration, aka Spatial normalisation FMRIB technical report TR07JA2 from www.fmrib.ox.ac.uk/analysis/techrep

[55] D. Rueckert, L. I. Sonoda, C. Hayes, D. L. G. Hill, M. O. Leach, and D. J. Hawkes. Non-rigid registration using free-form deformations: Application to breast MR images. IEEE Transactions on Medical Imaging, 18(8):712-721, 1999.

[56] Torgerson, C. M., Irimia, A., Leow, A. D., Bartzokis, G., Moody, T. D., Jennings, R. G., . . . Altshuler, L. L. (2013). *DTI tractography and white matter fiber tract characteristics in euthymic bipolar I patients and healthy control subjects*. Brain imaging and behavior, 7(2), 129-139.

[57] Xue, H., Shah, S., Greiser, A., Guetter, C., Littmann, A., Jolly, M. P., . . . Kellman, P. (2012). *Motion correction for myocardial T1 mapping using image registration with synthetic image estimation.* Magnetic resonance in medicine, 67(6), 1644-1655.

[58] Yamada, H., Abe, O., Shizukuishi, T., Kikuta, J., Shinozaki, T., Dezawa, K., . . . Imamura, Y. (2014). *Efficacy of distortion correction on diffusion imaging: comparison of FSL eddy and eddy_correct using 30 and 60 directions diffusion encoding*. PloS one, 9(11), e112411.

[59] Centre of Drug Research, Universiti Sains Malaysia (USM)

[60] Johnson, G. (2007). *Diffusion Tensor Imaging MRI for Abnormal Axonal Tracts*. Retrieved January 16, 2017, from http://braininjuryhelp.com/dti-diffusion-tensor-imaging-mri/

[61] Association Fiber. (2017). In Wikipedia, The Free Encyclopedia. Retrieved 08:23, April 17, 2017, from *https://en.wikipedia.org/wiki/Association_fiber*

[62] O'brien. (n.d.). *Nervous System 2*. Retrieved 08:23, April 17, 2017, from *https://www.studyblue.com/notes/note/n/nervous-system-2-2-23-2-25/deck/711090*

7.0 APPENDIX

new label, freesurfef label, freesurfer name
1, 2, "Left-Cerebral-White-Matter"
1, 41, "Right-Cerebral-White-Matter"
1, 77, "WM-hypointensities"
1, 85, "Optic-Chiasm"
1, 1004, "ctx-lh-corpuscallosum"
1, 2004, "ctx-rh-corpuscallosum"
2, 251, "CC_Posterior"
2, 252, "CC_Mid_Posterior"
2, 253, "CC_Central"
2, 254, "CC_Mid_Anterior"
2, 255, "CC_Anterior"
3, 1032, "ctx-lh-frontalpole"
4, 1014, "ctx-lh-medialorbitofrontal"
5, 1012, "ctx-lh-lateralorbitofrontal"
6, 1019, "ctx-lh-parsorbitalis"
7, 1020, "ctx-lh-parstriangularis"
8, 1018, "ctx-lh-parsopercularis"
9, 1027, "ctx-lh-rostralmiddlefrontal"
10, 1003, "ctx-lh-caudalmiddlefrontal"
11, 1028, "ctx-lh-superiorfrontal"
12, 1024, "ctx-lh-precentral"
13, 1017, "ctx-lh-paracentral"
14, 1035, "ctx-lh-insula"
15, 1026, "ctx-lh-rostralanteriorcingulate"
16, 1002, "ctx-lh-caudalanteriorcingulate"
17, 1023, "ctx-lh-posteriorcingulate"
18, 1010, "ctx-lh-isthmuscingulate"
19, 1006, "ctx-lh-entorhinal"
20, 1007, "ctx-lh-fusiform"
21, 1016, "ctx-lh-parahippocampal"
22, 1009, "ctx-lh-inferiortemporal"
23, 1033, "ctx-lh-temporalpole"
24, 1015, "ctx-lh-middletemporal"
25, 1030, "ctx-lh-superiortemporal"
26, 1034, "ctx-lh-transversetemporal"
27, 1001, "ctx-lh-bankssts"
28, 1022, "ctx-lh-postcentral"
29, 1031, "ctx-lh-supramarginal"
30, 1008, "ctx-lh-inferiorparietal"
31, 1029, "ctx-lh-superiorparietal"
32, 1025, "ctx-lh-precuneus"
33, 1005, "ctx-lh-cuneus"
34, 1011, "ctx-lh-lateraloccipital"
35, 1021, "ctx-lh-pericalcarine"

36, 1013, "ctx-lh-lingual"
37, 11, "Left-Caudate"
38, 12, "Left-Putamen"
39, 13, "Left-Pallidum"
40, 9, "Left-Thalamus"
41, 10, "Left-Thalamus-Proper"
42, 17, "Left-Hippocampus"
43, 18, "Left-Amygdala"
44, 26, "Left-Accumbens-area"
45, 28, "Left-VentralDC"
46, 2032, "ctx-rh-frontalpole"
47, 2014, "ctx-rh-medialorbitofrontal"
48, 2012, "ctx-rh-lateralorbitofrontal"
49, 2019, "ctx-rh-parsorbitalis"
50, 2020, "ctx-rh-parstriangularis"
51, 2018, "ctx-rh-parsopercularis"
52, 2027, "ctx-rh-rostralmiddlefrontal"
53, 2003, "ctx-rh-caudalmiddlefrontal"
54, 2028, "ctx-rh-superiorfrontal"
55, 2024, "ctx-rh-precentral"
56, 2017, "ctx-rh-paracentral"
57, 2035, "ctx-rh-insula"
58, 2026, "ctx-rh-rostralanteriorcingulate"
59, 2002, "ctx-rh-caudalanteriorcingulate"
60, 2023, "ctx-rh-posteriorcingulate"
61, 2010, "ctx-rh-isthmuscingulate"
62, 2006, "ctx-rh-entorhinal"
63, 2007, "ctx-rh-fusiform"
64, 2016, "ctx-rh-parahippocampal"
65, 2009, "ctx-rh-inferiortemporal"
66, 2033, "ctx-rh-temporalpole"
67, 2015, "ctx-rh-middletemporal"
68, 2030, "ctx-rh-superiortemporal"
69, 2034, "ctx-rh-transversetemporal"
70, 2001, "ctx-rh-bankssts"
71, 2022, "ctx-rh-postcentral"
72, 2031, "ctx-rh-supramarginal"
73, 2008, "ctx-rh-inferiorparietal"
74, 2029, "ctx-rh-superiorparietal"
75, 2025, "ctx-rh-precuneus"
76, 2005, "ctx-rh-cuneus"
77, 2011, "ctx-rh-lateraloccipital"
78, 2021, "ctx-rh-pericalcarine"
79, 2013, "ctx-rh-lingual"
80, 50, "Right-Caudate"
81, 51, "Right-Putamen"
82, 52, "Right-Pallidum"

83, 48, "Right-Thalamus"
84, 49, "Right-Thalamus-Proper"
85, 53, "Right-Hippocampus"
86, 54, "Right-Amygdala"
87, 58, "Right-Accumbens-area"
88, 60, "Right-VentralDC"